Digital Comprehensive Summaries of Uppsala Dissertations
from the Faculty of Science and Technology 2468

Dynamics of Solid Electrolyte Interphases in Li-ion Batteries

From Operando Analysis to Mechanistic Insights

TIM MELIN

ACTA UNIVERSITATIS
UPSALIENSIS
2024

ISSN 1651-6214
ISBN 978-91-513-2291-9
urn:nbn:se:uu:diva-540994

UPPSALA
UNIVERSITET

Dissertation presented at Uppsala University to be publicly examined in Häggsalen, Ångströmlaboratoriet, Lägerhyddsvägen 1, Uppsala, Thursday, 12 December 2024 at 09:15 for the degree of Doctor of Philosophy. The examination will be conducted in English. Faculty examiner: Professor Laurence Hardwick (University of Liverpool).

Abstract
Melin, T. 2024. Dynamics of Solid Electrolyte Interphases in Li-ion Batteries. From *Operando* Analysis to Mechanistic Insights. *Digital Comprehensive Summaries of Uppsala Dissertations from the Faculty of Science and Technology* 2468. 65 pp. Uppsala: Acta Universitatis Upsaliensis. ISBN 978-91-513-2291-9.

Li-ion batteries (LIBs) play a crucial role in the transition from fossil fuel to renewable energy sources by providing energy storage solutions for numerous applications. The modern high energy density LIBs were realised largely by the stabilisation of the electrode/electrolyte interface at the negative electrode with the solid electrolyte interphase (SEI). The SEI forms through electrolyte reduction during the first couple of charge/discharge cycles. Despite extensive optimisation of LIBs through electrolyte and SEI development, fundamental understanding of the formation, composition, structure and operating mechanism of the SEI is yet to be established. In order to address this gap, *operando* analytical techniques and model electrode/electrolyte systems were developed and applied to systematically investigate the formation and evolution of gaseous, soluble and solid reaction products. The thesis provides insights into the mechanisms behind SEI formation as driven by several important electrolyte solvents and additives, namely ethylene carbonate (EC), propylene carbonate (PC), vinylene carbonate (VC), lithium bis(oxalato)borate (LiBOB), 1,3,2-dioxathiolane 2,2-dioxide (DTD), and prop-1-ene-1,3-sultone (PES). Key findings include that EC and PC are reduced via identical reaction pathways, but with product of different solubilities, which in turn explains the difference in their ability to passivate the electrode surface. For the layer-forming additives, reduction pathways and their impact on the SEI passivation properties were identified and discussed. Although VC significantly reduces the layer thickness, the SEI is much denser and therefore more resistive to ion transport. LiBOB, DTD and PES were all found to have similar influence, namely passivate the electrode and suppress EC reduction, but each with their own peculiarities. LiBOB was found to be reduced already at 1.8 V vs. Li^+/Li to form primarily Li-oxalate based SEI along with electrolyte soluble borates. DTD reduces to primarily gaseous and solid products with a comparatively thicker SEI at 1.4 V vs. Li^+/Li. PES leads primarily to electrolyte-soluble product at 1.4 V vs. Li^+/Li, which in a subsequent step generates a comparatively thinner SEI. Both VC and PES reduced H_2 evolution, which was explained by the H_2O and H scavenging ability of their unsaturated carbon-carbon bonds. Based on the collective findings herein, an effective layer-former suppresses the reduction of both the electrolyte and its impurities and generates a 10 nm thick and dense SEI comprised primarily of inorganic Li-species. The insights into the SEI formation process on a fundamental level of the aforementioned solvents and additives showcase the ability of complementary *operando* analytical techniques to unravel the complexity of the elusive SEI. The insights thus gained guide the optimisation and development of electrolytes for current and future LIB chemistries.

Keywords: Li-ion batteries, Solid electrolyte interphase, Operando, Vibrational spectroscopy, Electrochemical quartz crystal microbalance, Online electrochemical mass spectrometry, Electrolytes, Additives

Tim Melin, Department of Chemistry - Ångström, Structural Chemistry, Box 538, Uppsala University, SE-751 21 Uppsala, Sweden.

ISSN 1651-6214
ISBN 978-91-513-2291-9
URN urn:nbn:se:uu:diva-540994 (http://urn.kb.se/resolve?urn=urn:nbn:se:uu:diva-540994)

”Det heter inte improvisera,
det heter forska när man inte vet vad man gör.”
– Kirurgerna, Magnus och Brasse

List of Papers

This thesis is based on the following papers, which are referred to in the text by their Roman numerals.

I. T. Melin, R. Lundström, E. J. Berg, "Revisiting the Ethylene Carbonate–Propylene Carbonate Mystery with Operando Characterization," *Adv. Mater. Interfaces*, vol. 9, no. 8, p. 2101258, 2022.

II. N. Gogoi, T. Melin, E. J. Berg, "Elucidating the Step-Wise Solid Electrolyte Interphase Formation in Lithium-Ion Batteries with Operando Raman Spectroscopy," *Adv. Mater. Interfaces*, vol. 9, no. 22, p. 2200945, 2022.

III. X. Hou, Tim Melin, V. Vanoppen, C. Li, M. Gaberscek, E. J. Berg, "The role of Vinylene Carbonate in Forming Dense Solid-electrolyte Interphase Species in Li-ion Batteries", *In manuscript*

IV. T. Melin, R. Lundström, E. J. Berg, "Elucidating the Reduction Mechanism of Lithium Bis(oxalato)borate," *J. Phys. Chem. Lett.*, vol. 15, no. 9, pp. 2537–2541, 2024.

V. T. Melin, R. Lundström, L. King, E. J. Berg, "Operando study of the reduction mechanism of sulfur-based layer-forming additives", *In manuscript*

Contributions to the papers

I. I planned the study together with E. J. Berg, performed all experimental work and wrote the manuscript with input from co-authors.

II. Shared first authorship with N. Gogoi. I took part in the planning, performed the experiments, and wrote the manuscript together with the co-authors. N. Gogoi and I contributed equally to the work.

III. Shared first authorship with X. Hou. Planned the study together with E. J. Berg, performed the experimental work and the analysis of the EQCM-D data together with H. Xu. Wrote the manuscript together with the co-authors. X. Hou and I contributed equally to the work.

IV. I planned the study and performed all experimental work except the OEMS measurements. I wrote the manuscript with input from the co-authors.

V. I planned and performed all experimental work. The OEMS data analysis was performed with input from R. Lundström. I wrote the manuscript with input from the co-authors.

Papers not included in the thesis

- R. Lundström, N. Gogoi, T. Melin, E. J. Berg, “Unveiling Reaction Pathways of Ethylene Carbonate and Vinylene Carbonate in Li-Ion Batteries,” *J. Phys. Chem. C*, vol. 128, no. 20, pp. 8147–8153, 2024.

- C. Misiewicz, A. Ulander, T. Melin, A. C. Hall, E. J. Berg, “Decoupling Degradation at the Electrode Interfaces in Prussian White Full Cells,” *Submitted*

Contents

Abbreviations

ATR	Attenuated total reflectance
CV	Cyclic voltammetry
DEC	Diethyl carbonate
DMC	Dimethyl carbonate
DME	1,2-dimethoxyethane
DTD	1,3,2-dioxathiolane 2,2-dioxide
EC	Ethylene carbonate
EG	Ethylene glycol
EIS	Electrochemical impedance spectroscopy
EQCM-D	Electrochemical quartz crystal microbalance with dissipation monitoring
EMC	Ethyl methyl carbonate
FTIR	Fourier transform infrared spectroscopy
GC	Glassy carbon
IRRAS	Infrared reflection absorption spectroscopy
LEDC	Lithium ethylene dicarbonate
LFP	$LiFePO_4$
LIB	Li-ion battery
LiBOB	Lithium bis(oxalato)borate
LPDC	Lithium propylene dicarbonate
LSV	Linear sweep voltammetry
mpe	mass per electron
NMC	Nickel manganese cobalt oxide
OCP	Open circuit potential
OEMS	Online electrochemical mass spectrometry
PC	Propylene carbonate
PEG	Polyethylene glycol
PES	Prop-1-ene-1,3-sultone
PPG	Polypropylene glycol
SEI	Solid electrolyte interphase
SEIRAS	Surface-enhanced infrared absorption spectroscopy
SERS	Surface-enhanced Raman spectroscopy
VC	Vinylene carbonate

1 Introduction

1.1 The role of Li-ion batteries in modern energy solutions

Over the past decade, the global energy consumption has increased from 161,000 TWh in 2013 to 183,000 TWh in 2023. Most energy produced is from fossil fuels, accounting for 81% of the energy production in 2013. Extensive efforts have been and are being made mainly for environmental and geopolitical reasons, which decreased fossil fuel reliance to 77% in 2023 [1]. Sustainable energy sources, mainly solar and wind, are gradually replacing fossil fuels. However, these energy sources are intermittent, often producing more energy than consumed during peak production. Conversely, they might not generate enough energy when the demand is high as the sun does not shine and the wind does not blow consistently. In order to match the supply and demand of energy, energy storage is necessary. Although pumped hydroelectric energy storage (PHES) is currently the dominating technique for grid balancing, the high capital cost and specific geographic conditions are restrictive [2]. Li-ion batteries (LIBs) have been introduced, both on an industrial and domestic scale, for grid balancing and stationary energy storage on timescale from seconds to hours. Compared to PHES, LIBs are more flexible and scalable, have faster response time, and lower environmental impact during operation [3].

In parallel to the energy production sector, the transport sector is also going through major electrification from internal combustion engine (ICE) vehicles to battery electric vehicles (BEVs), driven by the same environmental and geopolitical reasons. For these applications, LIBs are the most appropriate battery chemistry due to their high power and energy density, as well as their long cycle life.

In addition to the applications discussed above, LIBs are the batteries exclusively used in portable electronic devices including laptops, phones, and tablets. Consequently, multiple sectors are heavily invested and reliant on LIBs, leading to a market likely to further grow significantly in the coming decade. Continuous advancements of LIBs are crucial to meet the growing demand for sustainable energy.

1.2 Li-ion batteries

The first LIB was commercially introduced in 1991 by Sony. The negative and positive electrodes were comprised of petroleum coke and lithium cobalt oxide ($LiCoO_2$), and the electrolyte was carbonate ester-based. Almost 30 years after the commercialisation, the pioneers who contributed with vital research leading to the success of LIB, John B. Goodenough, M. Stanley Whittingham and Akira Yoshino were awarded the 2019 Nobel Prize in Chemistry [4]. Major advancements have been made since the first LIB and the performance in terms of energy and power density, cycle life, and safety has enabled the implementation of LIBs in various applications. Despite the significantly improved performance, the electrode materials and electrolyte solutions in modern LIBs have remained fairly similar to those of the initial LIB.

A typical modern LIB consists of a mixed metal oxide, e.g. nickel manganese cobalt oxide (NMC), as the positive electrode, graphite as the negative electrode, and an electrolyte solution of $LiPF_6$ dissolved in a mix of carbonate esters [5]. In order to avoid electrical short-circuiting the electrodes, a separator made of porous polypropylene/polyethylene film is placed between the electrodes. The whole electrode-separator-electrode stack is soaked in electrolyte. Figure 1.1 shows a schematic representation of a LIB during discharge.

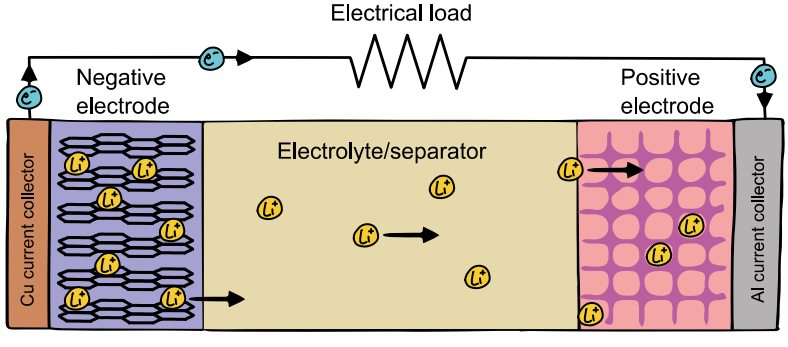

Figure 1.1. Schematics of a Li-ion battery during discharge.

LIBs are secondary batteries, i.e. rechargeable, and as the name indicates Li^+-ions play a crucial role. When fully charged, Li^+-ions occupy sites between the graphene layers of the negative graphite electrode while the sites between the transition metal oxide layers of the positive electrode are empty. The redox potential of the negative electrode is lower than the redox potential of the positive electrode, meaning that when the external circuit is closed, the spontaneous reaction is oxidation of the negative electrode, de-intercalation of Li^+-ions, and reduction of the positive electrode, intercalation of Li^+ into the empty sites. During discharge, Li^+-ions and electrons move from the negative electrode to the positive electrode, maintaining charge neutrality. Li^+-ions travel

through the electrolyte, while electrons flow through the external circuit. During charge, an external current is applied in the opposite direction, i.e. the arrows in Figure 1.1 are reversed and oxidation of the positive electrode and reduction of the negative electrode occurs.

1.2.1 The negative electrode

The largely uncontested negative electrode material in LIBs is graphite, a crystalline allotrope of carbon, and comprised of stacked graphene layers. When applying a sufficiently low potential, <0.2 V vs. Li^+/Li, the graphite is reduced and Li^+-ions intercalate in between the layers until the Li^+-ions to carbon atoms ratio is 1:6, equal to a specific charge of 372 mAh g^{-1} [5].

Alternatives to graphite have been sought after and researched extensively. Silicon, the dominating semiconductor material used in electronics, can be lithiated to a degree much higher than graphite. Through an electrochemical alloying reaction, the theoretical maximum specific charge is one order of magnitude higher than for graphite (4200 mAh g^{-1}). However, silicon electrodes suffer from several challenges, most commonly attributed to the significant volume expansion during lithiation (>300 vol.%) [6]. To circumvent this, the particle size of the electrode material can be reduced. High-energy Li-ion cells today often contain graphite electrodes doped with silicon nanoparticles (5-10 wt.%). Lithium metal is regarded as the *Holy grail* for negative electrode materials in the battery field. Li-metal has a specific charge of 3860 mAh g^{-1} and a redox potential of 0 V vs. Li^+/Li (-3.04 V vs. standard hydrogen electrode), which is the highest possible capacity and lowest redox potential of any electrode material utilising Li^+-ions. However, Li-metal anodes suffer from formation of highly porous structures during repeated charge/discharge cycles which ultimately leads to loss of active material and capacity loss [7].

Among the numerous requirements an electrode material has to fulfil to be considered a reasonable choice, e.g. reversible redox reaction involving Li^+-ions, sufficient electronic conductivity, chemical and mechanical stability, the electrochemical stability towards the electrolyte is arguably the most important.

1.2.2 The electrolyte

The main function of an electrolyte solution used in any electrochemical system is to transport ions between the negative and positive electrodes with the same flux as the electrons in the external circuit. An electrolyte solution can be either liquid or solid, and both types are used in LIBs. Liquid LIB electrolytes typically comprise a lithium salt dissolved in an organic solvent. Solid electrolytes may consist of a lithium salt dissolved in a polymer (typically polyethylene oxide) or a Li^+-ion conducting ceramic. The predominant electrolyte in LIBs, shown in Figure 1.2, is lithium hexafluorophosphate ($LiPF_6$)

dissolved in a mix of ethylene carbonate (EC) and linear alkyl carbonate esters (e.g. dimethyl carbonate (DMC), diethyl carbonate (DEC), or ethyl methyl carbonate (EMC), or combinations thereof) [8].

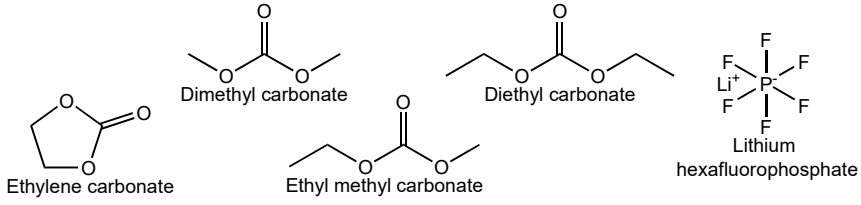

Figure 1.2. Structures of the most common electrolyte salt and solvents used in Li-ion batteries.

Solvent mixtures are applied to the enhance ionic conductivity (~8 mS cm^{-1} at 25°C for 1 M $LiPF_6$ in EC:DEC, 1:1 volume ratio), yet provide acceptable anodic and cathodic stability and wide liquid temperature ranges. While there are alternative salts, $LiPF_6$ displays the desirable ability to passivate the aluminium current collector of the positive electrode. Aluminium corrosion is detrimental and if no passivation occurs, the battery performance rapidly decays as the current collector deteriorates. The high dielectric permittivity of EC provides a high salt solubility and dissociation whereas the linear carbonate esters lower the electrolyte viscosity and enhances Li^+-ion mobility. Additionally, linear carbonate esters have low melting points (-74°C for DEC), broadening the liquid temperature range [9]. Carbonate esters and $LiPF_6$ have high anodic stability and most cathode materials have redox potentials below the oxidation of the electrolyte solution. The cathodic stability of PF_6^- is not usually discussed, and is assumed to be not be an issue. However, PF_6^- easily destabilises in the presence of H^+ and H_2O, which leads to chemical decomposition to PF_5 and HF (Reaction 1.1). $LiPF_6$ hydrolysis yields HF, POF_3, and LiF (Reaction 1.2) [10]. These products are reactive towards electrolyte and electrode components. Therefore, keeping the battery essentially water-free is important and rigorous drying of all components is a crucial step in LIB manufacturing.

$$H^+/Li^+ + PF_6^- \rightleftharpoons PF_5 + HF/LiF \quad (1.1)$$

$$LiPF_6 + H_2O \rightarrow LiF + POF_3 + 2HF \quad (1.2)$$

Water is not only problematic for the $LiPF_6$, but also for the carbonate esters, mainly EC. EC hydrolysis driven by only water is comparatively slow at normal operating temperatures (around room temperature) and is not considered a major issue. However, water reduction, starting at 1.8 V vs. Li^+/Li (Reaction

1.3), results in hydroxide ions which catalyse the hydrolysis (Reaction 1.4). Hydrolysis of EC leads to an autocatalytic ring-opening reaction forming polyethylene glycol (PEG). PEG could be detrimental to the electrolyte conductivity as it increases the electrolyte viscosity [11].

$$H_2O + e^- \rightarrow \frac{1}{2} H_2 + OH^- \quad (1.3)$$

$$OH^- + n\,EC \rightarrow n\,CO_2 + [PEG]_n^- \quad (1.4)$$

The cathodic stabilities of carbonate esters are similar within the group, with a reduction potential below 0.8 V vs. Li^+/Li for EC and DEC on carbon electrodes. Notably, the reduction of carbonate esters occurs at higher potentials than the onset of Li^+ intercalation into graphite. Yet, carbonate esters are used successfully with graphite electrodes for 1000's of charge/discharge cycles. This is possible since the reduction of EC produces species that passivate the graphite surface, creating a solid electrolyte interphase (SEI), which limits further electrolyte reduction [12].

1.2.3 Additives

Though making up a relatively small part of the overall battery cell (typically ~5 wt.% of the electrolyte which equals to less than 1 wt.% of the total cell), electrolyte additives play an important role. Numerous additives are used in LIBs for various tasks, and these can be divided into different types based on their function. Stabilisers are molecules that for example slow down the degradation of PF_6^- [13], or transesterification of the linear carbonate esters. Flame-retardants, usually phosphorous-based or heavily fluorinated molecules (e.g. triethyl phosphate and hydrofluoroethers) are added to the electrolyte to suppress the flammability of the carbonate esters [14]. The function of scavengers is to "clean up" the battery from unwanted species before they interfere with the electrodes or lead to side reactions. A typical unwanted species is water, and common water-scavenging additives are organosilicon compounds (e.g. tris(trimethylsilyl)phosphate) [15].

Arguably the most important type of additives are layer-forming additives, with the task of forming passivating layers on the positive and negative electrode surfaces. As new positive electrode materials are developed with higher redox potentials, additives forming passivation layers when oxidised, e.g. tris(trimethylsilyl) phosphite and fluoroethylene carbonate, are getting more and more attention. Traditionally, layer-forming additives have received more attention than other additive types, as they play a crucial role in stabilising the electrode-electrolyte interphase which in turn enables reversible charge and discharge cycles. In this thesis, the reduction of EC and layer formation of four SEI-forming additives, vinylene carbonate (VC), lithium

bis(oxalato)borate (LiBOB), 1,3,2-dioxathiolane 2,2-dioxide (DTD) and prop-1-ene-1,3-sultone (PES) are studied in detail (see the structures in Figure 1.3).

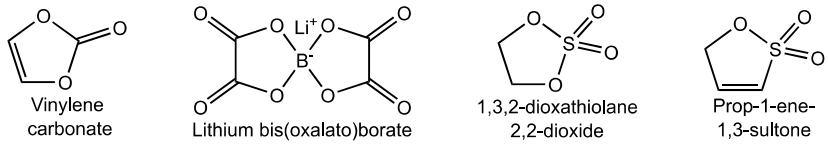

Figure 1.3. Structures of the layer-forming additives studied in this thesis.

1.3 The solid electrolyte interphase

1.3.1 The SEI model

The solid electrolyte interphase, SEI, is a three-dimensional phase between the solid electrode and the liquid electrolyte. The term was coined in 1979 by Peled when studying nonaqueous battery systems with alkali and alkaline earth metals as negative electrodes [16]. The SEI was described as a layer comprised of insoluble species which formed as the metal electrodes came in contact with the electrolyte. Peled emphasised the significance of the SEI for non-aqueous batteries, noting that improving performance requires control over the SEI and its properties, such as resistivity. This statement still stands and is equally true today as it was over four decades ago. Following this study, the SEI concept was adapted to carbon electrodes used in Li-ion batteries [12]. Figure 1.4 shows the two most widely accepted models used to describe the SEI, the mosaic model presented by Peled [17] and the layered model presented by Aurbach [18]. In both models, the SEI is formed by irreversible electrolyte reduction during the first charge and discharge cycles and contains both organic and inorganic species. In the former model, species are heterogeneously mixed in a mosaic-like structure. In the latter model, the inorganic species are densely packed closest to the electrode and the organic species form a porous part.

The composition of the SEI has been the subject of countless studies and a variety of species have been found. LiF has been found to be an SEI constituent in almost all $LiPF_6$-based electrolytes. Not only the SEI composition is under debate, but also the importance of different species. In some studies, LiF is regarded as a key component. In other studies, LiF is claimed to be a poor Li^+-ion conductor and Li_2CO_3 is believed to be important to obtain a functional SEI. These disparities in the composition and importance of different species may be attributed to two main factors. Firstly, the SEI composition is highly dependent on the electrolyte formulation and even if the same salt and solvents are used, minute variations in contaminant levels could greatly

impact the SEI formation process and composition. Secondly, the SEI is mostly analysed with *ex situ* techniques. This means that. the electrode on which the SEI has formed must be extracted by disassembling the battery after cycling, washed to remove electrolyte residues, and transferred to the instrument for analysis. SEI species are often metastable and reactive to ambient atmosphere, contaminants present in the glovebox (where the samples are prepared) or the solvent used for washing. The solubility of the species might also vary and preferential dissolution of some species could occur during washing. In addition to the stability issues of the SEI, its thickness is only a few nanometres and therefore difficult to analyse with most techniques.

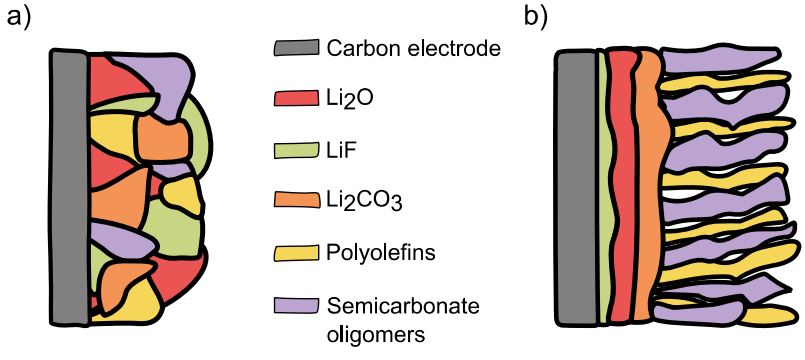

Figure 1.4. The two most widely accepted models of the solid electrolyte interphase (SEI), a) the mosaic model and b) the layered model.

Despite the confusion regarding its composition, consensus on the essential properties of the SEI is well-established. For a functional battery, the SEI must have sufficient Li^+-ion conductivity to facilitate Li^+-ion transport between the electrode and electrolyte during charge and discharge. Poor Li^+-ion conductivity results in large overpotentials, poor energy efficiency and heat generation which is detrimental to the battery. Secondly, it must be electronically insulating to hinder electron transfer from the electrode to the electrolyte. Lastly, the SEI must exhibit both chemical and mechanical stability. Chemically, it should resist dissolution and reactions with the electrolyte. Mechanically, it must withstand cracking and delamination caused by the expansion and contraction of the electrode during cycles of charge and discharge. If the SEI lacks the latter two properties, continuous irreversible reactions, i.e. electrolyte reduction, would occur leading to fast capacity fade of the battery. A crucial component to obtain all these properties is as mentioned in section 1.2.3, layer-forming additives.

1.3.2 *Ex situ* analysis of the SEI

Analysis and characterisation of the solid electrolyte interphase is notoriously challenging due to its nanoscale dimensions and chemical instability. In this section, *ex situ* X-ray photoelectron spectroscopy (XPS) and Fourier transform infrared spectroscopy (FTIR), data are presented and compared. While these two techniques are not exclusively used for analysing the SEI, they are among the most commonly employed techniques and can be used to illustrate the possibilities and challenges associated with *ex situ* analysis of the SEI [19]. XPS is routinely used within the LIB field to study electrode surfaces and has helped gain important insights into interfacial chemistry. The probing depth is typically a few nanometres, ideal for studying the SEI. Elemental composition and chemical state of different elements can be obtained, and in combination with the extensive amount of reference XPS spectra, many species, both organic and inorganic can be characterised. In some cases, depth profiling by tuning the incident photon energy or ion etching is possible. However, the challenges of XPS are that the high energy X-ray photons can cause radiation damage leading to the decomposition of the SEI. Furthermore, the analysis is performed *ex situ*, which entails the challenges of sample preparation briefly discussed in section 1.3. Samples of the cycled electrodes have to be extracted in an Ar-filled glovebox and washed with an appropriate solvent minimise transformation or dissolution of the SEI species. After washing, the samples have to be dry and not include any volatile solids since XPS is performed under ultra-high vacuum. Having solvents or volatile solids evaporating in the spectrometer would not only interfere with the recorded spectra but could also be detrimental to the instrument. In the spectrometer, charging effects caused by the ejection of photoelectrons can occur if the sample is non-conductive resulting in shifts in the peaks seen in the spectra.

FTIR is another widely used *ex situ* technique used to analyse electrode surfaces in LIBs, and it is often used as a complementary technique to XPS. Unlike to XPS, ultra-high vacuum is not needed and there are different modes of measuring making different types of samples possible to analyse. Sample preparation is still needed but the dryness of the samples is not essential as for XPS. The most suitable measuring mode is attenuated total reflectance (ATR-FTIR) since it does not require the samples to be IR transparent or reflective. The analysis depth in ATR-FTIR is highly dependent on the wavelength of the incident IR light, the setup, and the sample's refractive index, but is usually a couple of micrometres. The obtained spectra show vibrational bands specific to functional groups and molecules making it ideal for characterising SEI species. Even though there is an immense literature on reference spectra for different molecules, identification of SEI species is often challenging due to overlapping bands from electrolyte components with structures similar to the SEI species.

There are, of course, a plethora of additional useful techniques to study the SEI *ex situ*, including scanning and transmission electron microscopy (SEM and TEM), atomic force microscopy (AFM), nuclear magnetic resonance (NMR), X-ray diffraction (XRD) and many others. These techniques can give a good idea of how the SEI is structured and its composition. However, as mentioned in this thesis, some sort of sample preparation is needed before analysis, which potentially could alter the SEI composition and give a false picture of the SEI and its formation processes.

1.3.3 *In situ/operando* analysis of the SEI

In order to gain further insights into the SEI formation and its composition, real-time observations under the formation processes, i.e. *in situ* and *operando* techniques, are needed. *In situ* and *operando*, meaning "on site" and "during operation", describe analysis techniques performed on battery cells without disassembling or during charge/discharge cycles. A single technique is not enough to gain a comprehensive understanding of the SEI, a combination of *in situ*/*operando* techniques that can probe different phases is needed. Hence, the number of different *operando* techniques used in SEI studies is extensive, showcasing the importance of real-time observations. The result is a copious and seemingly inexhaustible amount of literature, subject to numerous reviews [20], [21], [22], [23], [24], [25]. The following paragraphs present the background and significance of the techniques utilised in this thesis.

In situ vibrational spectroscopy for studying interphases in LIB-relevant systems was pioneered in the early 1990s by Aurbach and co-workers showcasing the possibilities of *in situ* FTIR [26], [27]. Two setups were presented, one for single reflectance IR spectroscopy using an IR transparent NaCl crystal and the other for an ATR-FTIR configuration using a ZnSe ATR crystal. Both crystals were coated with a thin layer of a noble metal (Pt) and used as a working electrode as well as a reflection element. On top of the metal-coated side, an electrochemical cell was mounted. Due to the internal reflection, an evanescent wave forms and the IR light can interact with the layer closest to the metal layer before reaching the electrolyte circumventing the issue of overlapping electrolyte solvent vibration bands in spectra recorded with setups based on external reflectance. In light of this study, development and improvements on *in situ* FTIR began by Novák [28], [29] among others. In the early 2000s, the idea of replacing the carbonate esters with another solvent with less vibrational overlap with the SEI species was introduced. Ross and co-workers studied EC reduction in a model electrolyte based on tetrahydrofuran (THF) with *ex situ* FTIR [30]. This concept was later adopted and applied to study the reduction of vinylene additives with *in situ* FTIR [31], [32]. In recent years, *in situ* ATR-FTIR has been employed to study SEI formation on Si electrodes [33], [34], [35]. Another promising FTIR configuration is surface-enhanced infrared absorption spectroscopy (SEIRAS). This setup is identical

to the aforementioned *in situ* ATR-FTIR setup but includes a nanostructured noble metal film. The evanescent wave of IR light excites localised surface plasmons resulting in an enhanced interaction between the analyte in the closest vicinity of the nanostructure and the light. SEIRAS has been used to study lithium-oxygen battery systems [36], [37], [38]. However, the technique is yet to be utilised successfully to study the SEI.

In parallel to FTIR, *in situ* Raman spectroscopy was used for studying interphases and bulk electrode properties in similar systems. In 1992, Odziemkowaski et al. employed *in situ* Raman spectroscopy to study the interphase formed on Li-metal electrodes in a $LiAsF_6$-THF electrolyte [39]. In the following years, *in situ* Raman spectroscopy was utilised to study Li^+-ion intercalation into graphite [40], [41], [42]. Surface-enhanced Raman spectroscopy (SERS) has been developed and used successfully for studying SEI formation [43], [44], [45], [46]. The success of SERS is most likely due to significantly stronger enhancement compared to SEIRAS.

The first electrochemical quartz crystal microbalance (EQCM) study on SEI formation was performed by Aurbach et al. in 1995. Reduction of propylene carbonate (PC)-based electrolytes with $LiAsF_6$ and $LiPF_6$ as well as the effect of water and CO_2 contamination was studied [47]. More recent work was performed by Kitz et al., in which EQCM with dissipation monitoring (EQCM-D) was employed to study interphase formation in common LIB electrolytes [11], [48], [49]. In EQCM-D, multiple overtones and the dissipation of each are recorded, enabling advanced models to be fitted to the data from where e.g. viscoelastic properties are obtained. The setup developed in these studies is used in this thesis.

Online electrochemical mass spectrometry (OEMS) is a group of techniques used for *in situ* and *operando* gas analysis of electrochemical systems. Contrary to the definition of OEMS, setups where all evolved gas is extracted through a membrane in contact with the electrode or electrolyte are commonly referred to as differential electrochemical mass spectrometry (DEMS), while setups where the evolved gas accumulates in a headspace from which it is sampled are referred to as OEMS. The first *in situ* gas analysis studies on LIB electrolyte reduction were performed at the end of the 1990s by Imhof and Novák [28], [50]. They showed with a DEMS setup that EC and PC are reduced below 0.8 V vs. Li^+/Li with ethylene and propylene as gaseous products. Multiple iterations of new and improved OEMS setups suitable for studying SEI formation have been presented [51], [52], [53], most recently by Lundström and Berg [54].

2 Scope of the thesis

This thesis investigates the formation processes and composition of the solid electrolyte interphase (SEI) derived from ethylene carbonate and various additives, including VC, LiBOB, DTD, and PES. To capture the elusive interfacial processes occurring at the electrode surfaces in LIBs, OEMS, *operando* Vibrational spectroscopy and EQCM are utilised to probe gaseous, liquid, and solid phase products.

In **Paper I**, the "EC-PC mystery" is revisited with OEMS and EQCM-D to investigate the reason for the difference in SEI stability derived from the two solvents. In this study, virtually identical reduction pathways were observed for EC and PC. The main difference was found in the solubility of the SEI where the EC-derived layer passivated the electrode and remained stable while the PC-derived layer dissolved as soon as the cycling was stopped. The reduction of EC was further investigated in **paper II** with *operando* Raman spectroscopy and OEMS. Additional findings in this study were that contaminants, such as O_2, CO_2 and H_2O greatly impact the initial interphase formation.

Paper III investigates the reduction of EC in a DEC-based electrolyte with and without the presence of VC. In this study, EQCM-D coupled with EIS showed continuous growth of the SEI when only EC was present, stemming from water reduction. A less charge-consuming and faster SEI formation was observed with only minute amounts (1-3 vol.% VC) in the electrolyte, showcasing the effectiveness of VC as an additive.

In **Papers IV** and **V**, the reduction mechanisms of three additives, LiBOB, DTD and PES, are studied in detail with *operando* ATR-FTIR, OEMS and EQCM in an ether-based model electrolyte. It was shown that all three additives can passivate the electrode surface and thus hinder EC reduction, while only LiBOB and PES suppress H_2O evolution from water reduction.

The findings in this thesis demonstrate the power of *operando* techniques and the importance of their continuous development to get a more complete fundamental understanding of the SEI formation processes and composition in LIBs.

3 Methodology

In this thesis, four different *operando* techniques are developed and applied to study SEI formation. Each technique is chosen to analyse reduction products in different phases. Gaseous, soluble, and solid products are monitored with online electrochemical mass spectrometry (OEMS), *operando* attenuated total reflectance Fourier transform infrared spectroscopy (ATR-FTIR) and surface-enhanced Raman spectroscopy (SERS), as well as electrochemical quartz crystal microbalance with dissipation monitoring (EQCM-D).

3.1 Model systems

Model systems of varying types are used in **Papers I-V**. A model system is defined as a system carefully designed to single out one or a couple of processes only which otherwise occur among many others in complex systems, e.g. in LIBs. In this thesis, the model systems are carefully chosen to decrease the number of components interfering with or overlapping the SEI processes.

In **Papers I**, **IV** and **V,** to minimise the effects of Li^+-ion (and solvent co-) intercalation and facilitate clearer detection of passivation of the electrodes, glassy carbon electrodes are used instead of graphite electrodes. Moreover, in **Paper I**, $LiClO_4$ is used as electrolyte salt to minimise the effects of the chemical decomposition of $LiPF_6$. To isolate the reduction processes of the layer-forming additives in **Papers IV** and **V**, 1,2-dimethoxyethane (DME) is used as a single-solvent model electrolyte.

To ensure control over the working electrode potential, Li-metal is commonly used as a combined counter and reference electrode, assuming that its redox potential is fixed at 0 V vs. Li^+/Li. However, Li-metal is not optimal due its reactivity towards the electrolyte resulting in unwanted species and drift of its redox potential. These species can diffuse to the working electrode affecting the SEI formation. Therefore, $LiFePO_4$ (LFP) is used as counter electrode (and reference electrode in the EQCM cell) in all measurements except the *operando* SERS measurements in **Paper I**. To ensure a stable redox potential, the LFP electrodes are delithiated to 80% of their initial capacity where the redox plateau at 3.43 V vs. Li^+/Li is reached before being used as counter/reference electrodes. Considering the comparatively small charge extracted from the LFP (roughly 10% of the total charge during the first negative

polarisation of a porous glassy carbon electrode), the potential of the LFP is to a first approximation assumed to be constant throughout all experiments, hence acting as a combined counter and reference electrode.

In lab-scale battery cells, an excess amount of electrolyte is commonly used to ensure proper wetting of the electrodes. This contrasts with commercial cells, where the electrolyte amount is minimised to reduce weight and cost. In *operando* cells, this excess becomes even more pronounced due to additional requirements regarding the cell geometry. This significantly influences the effect of contaminants on SEI formation, as more unwanted reactions occur on the electrode surface and increases the risk of dissolution of solid SEI species. Therefore, the ratio between electrode surface area and electrolyte volume, known as the flooding factor, is a crucial parameter to consider when developing and applying *operando* setups.

3.2 ATR-FTIR

Infrared spectroscopy principally operates by recording the interaction of infrared (IR) light with molecules. When a sample is irradiated by IR light it absorbs specific parts of the incident light matching the energy of vibrational modes of the sample molecules. The energy of the absorbed light is molecule-specific and the transmitted or reflected spectrum can be used to identify the sample molecules [55]. Figure 3.1 shows a schematic of the essential parts of the two-electrode electrochemical ATR-FTIR cell used in **Papers IV** and **V**. The electrolyte volume used in all ATR-FTIR measurements was 100 µL. The surface area of the electrodes used was 100-200 cm^2, resulting in a flooding factor of 0.5-1 µL cm^{-2}.

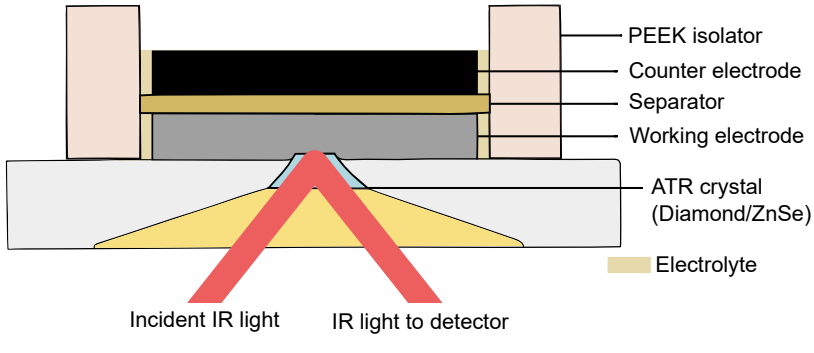

Figure 3.1. Schematics of the two-electrode electrochemical ATR-FTIR cell.

ATR-FTIR is based on the total internal reflection of IR light in a high refractive index crystal. For internal reflection to occur, the angle of incidence has

to be equal to or greater than the critical angle, Θ_c which is dependent on the refractive indices of the crystal and the sample according to equation 3.1.

$$\theta_c = sin^{-1}\frac{n_2}{n_1} \tag{3.1}$$

When the light is reflected at the crystal-sample interface, an evanescent wave orthogonal to the interface is formed. The penetration depth (d_p) of the evanescent wave can be calculated by equation 3.2,

$$d_p = \frac{\lambda}{2\pi(n_1^2 sin^2\theta - n_2^2)^{1/2}} \tag{3.2}$$

where λ is the wavelength of the light, and Θ the angle of the incident light relative to the normal of the crystal surface [56]. High refractive index crystals, e.g. ZnSe, Ge and diamond, are preferable since they enable analysis of samples with lower refractive index. However, not only the refractive index is an important aspect to consider when designing an *operando* ATR-FTIR cell but also the chemical stability. During polarisation of the working electrode, which is pressed against the ATR crystal, the local environment might become acidic or alkaline, which is problematic for ZnSe and Ge as they will dissolve or decompose. In addition, both ZnSe and Ge can be lithiated at low potentials [57], [58]. Diamond, on the other hand, has excellent chemical and mechanical stability but a refractive index of 2.4, lower than the refractive index of glassy carbon and graphite. Despite this, it can still be used as an ATR crystal in the *operando* ATR-FTIR cell since the glassy carbon working electrodes are porous and most of the analysed volume was dominated by the electrolyte within the pores.

3.3 SERS

Figure 3.2 shows a schematic illustration of the *operando* Raman spectroscopy cell used in **Paper I**. The working electrode is a commercial SERS substrate made of Au-coated Si-nanopillars [59]. The electrolyte volume used in the SERS measurements was 50 µL and the estimated surface area, based on the capacitive current estimated around OCP, was 10 cm^2, which yields a flooding factor of 5 µL cm^{-2}. Note that the estimated surface area is roughly 100 times larger than the geometrical area of the SERS substrate (0.09 cm^2).

The operating principle of Raman spectroscopy is similar to IR spectroscopy as both obtain a spectrum featuring the vibrational modes of a molecule or material. However, Raman spectroscopy is based on the inelastic scattering of monochromatic light. When irradiating the sample, molecules can be excited to virtual energy states [55]. During relaxation, the excited molecules

transition back to their ground state, while a small fraction transitions to a vibrational energy state. The lost energy of the inelastically scattered light is equal to the energy of the vibrational state. By using monochromatic incident light, the scattered spectrum can be adjusted accordingly to the incident wavelength, giving a spectrum of the vibrational modes. The probing depth is a few micrometres (depending on the material, laser wavelength and the microscope) and to achieve surface sensitivity, a nanostructured Au substrate can be used. The nanostructure of the Au substrate enables enhanced Raman scattering of molecules near or adsorbed to the surface. The enhancement is caused by laser-excited localised surface plasmons resulting in an amplified localised electric field which in turn amplifies the Raman scattered light. Another enhancement theory is that the interaction between the incident laser and Au enables charge transfer between absorbed molecules and the Au, increasing the adsorbates' polarisability, i.e. increasing the Raman scattering [60]. The SERS effect is limited to a couple of metals where Au is the most preferred one.

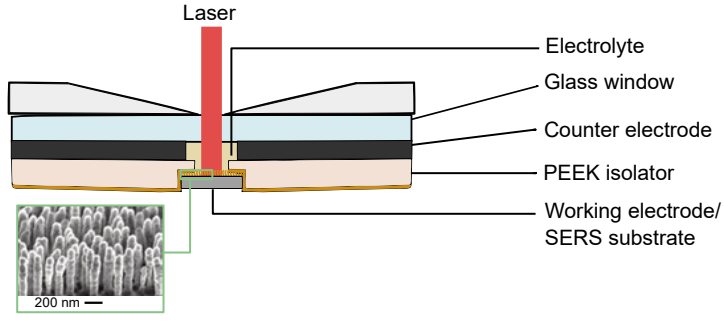

Figure 3.2. Schematics of the *operando* Raman spectroscopy cell with an inset electron micrograph (bottom left) of the Au nanopillars (adapted from [59]).

3.4 EQCM-D

Figure 3.3 shows the EQCM-D cell used in this work. The QCM sensor, used as a working electrode is a piezoelectric AT-cut quartz crystal with a resonance frequency of 5 MHz. The quartz is coated with two thin electrodes between which an alternating electric field is induced. This results in an oscillation of the quartz crystal [61]. The top electrode on the QCM sensor (Au or carbon as the outermost layer) is used as a working electrode and contacted through the QCM electronics. The reference electrode is placed on the mesh above the sensor which is in contact with the cell body. The counter electrode is in contact with the lid by a stainless-steel spring. The electrolyte volume in this cell is 450 µL and the sensor area in contact with the electrolyte is 1.13 cm^2, yielding a flooding factor of 400 µL cm^{-2}.

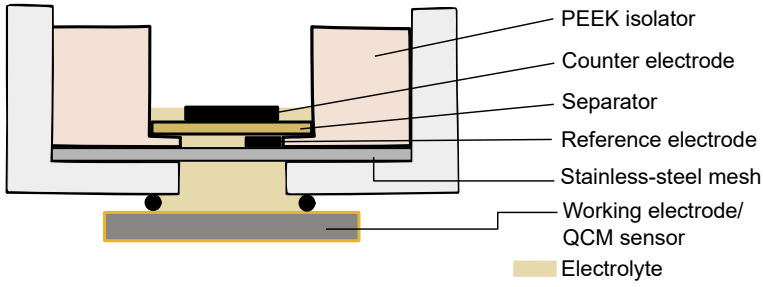

Figure 3.3. Schematics of the EQCM-D cell.

The oscillation induced by the alternating electric field applied over the quartz crystal induces an acoustic wave travelling across the thickness of the crystal and is reflected at its surfaces. Resonance is reached when the wavelength of the acoustic wavelength is equal to an uneven multiple of the sensor's thickness. If a homogenous rigid, and thin layer is deposited onto the sensor, a decrease of the resonance frequency occurs. Assuming that the deposited layer has similar acoustic properties as quartz, the atom displacement and shear stresses are continuous through the sensor-film interface, i.e. the "no-slip condition" is fulfilled, the relation between the change in mass, Δm, and resonance frequency, $\Delta f_{r,n}$, can be described by the Sauerbrey equation (equation 3.3),

$$\frac{\Delta m}{A} = -C_{SB}\frac{\Delta f_{r,n}}{n} \tag{3.3}$$

where C_{SB} is the Sauerbrey constant which can be calculated from the mechanical properties of the quartz crystal, A is the piezoelectric active surface area, and n is the overtone order [62]. The combination of QCM and electrochemistry enables *operando* monitoring of the mass increase per electron value (mpe-value). However, to confidently use the Sauerbrey equation, the layers deposited on the sensors have to be rigid. The SEI, a mix of inorganic and organic species, do not fulfil this requirement as it possesses non-rigid viscoelastic mechanical properties. The non-rigidity causes dampening of the acoustic wave. Monitoring the shift in frequency and dissipation of multiple overtones enables the viscoelastic properties of the SEI to be obtained with the Voigt model [61]. The model fits shifts in frequency and dissipation to a model based on the density, thickness, viscosity and shear modulus of the layer, and the density and viscosity of the liquid in the vicinity of the layer. The Voigt model has been used studying the viscoelastic properties of the SEI in LIB systems and has led to many important insights [11], [48], [49], [63], [64].

3.5 OEMS

Figure 3.4 shows the schematic of the OEMS cell without the stainless-steel body, lid and springs, and the valves connecting the cell to the mass spectrometer, pressure sensor, pump, and Ar gas cylinder. Above the electrode stack, there is a gas headspace of roughly 6 mL, where the evolving gases from the interphase reactions accumulate. Gas sampling from and purging (refilling with pure Ar) of the headspace is done intermittently. The working electrodes used in this setup must allow the evolved gas to diffuse through the electrode to reach the headspace, therefore stainless-steel mesh is used instead of Cu-foil as current collector for the working electrode. Except for the Au-sputter coated mesh electrode used in **Paper II**, the electrodes had a surface area of 100-300 cm^2. The electrolyte volume used in the OEMS measurements was 150-300 µL, resulting in a flooding factor of 0.75-2 µL cm^{-2}.

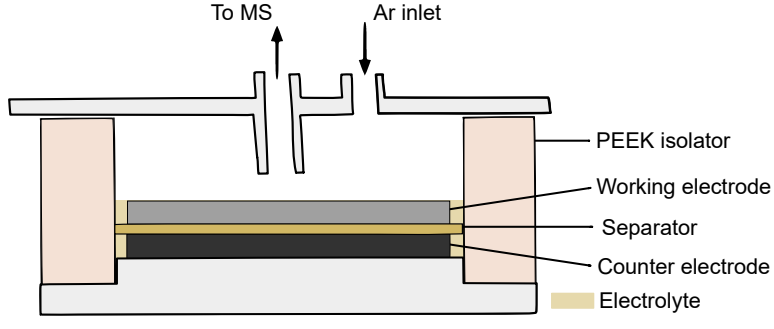

Figure 3.4. Schematics of the OEMS cell.

The sampled gas is led to the mass spectrometer. In the mass spectrometer, the gas is ionised (by electron ionisation) followed by filtering of the ionised fragments based on their mass-to-charge ratio (m/z) before reaching the detector (electron multiplier). By scanning the filter, the ion currents of different fragments with different m/z values reach the detector and a mass spectrum can be recorded. The mass spectrum is then compared to reference spectra to identify the gas species. By recording the mass spectra of known calibration gases with known compositions, exact ratios of different gas species can be obtained. Gas evolution rates of a reaction, e.g. SEI formation, can be obtained by sampling a known gas volume at a known rate. A detailed description of the setup, calibration and data processing can be found in the following publication by Lundström [54].

4 SEI formation in LIBs

4.1 EC, PC and VC

The SEI is regarded as the most critical component that has a decisive role in the performance and longevity of LIBs. EC is often praised for its ability to form a stable SEI on graphite electrodes hindering further electrolyte reduction while maintaining sufficient Li^+-ion transport between the electrolyte and electrode. Despite the widespread use of EC and numerous studies of EC-derived SEI, the reduction pathway is not fully understood. Besides EC, two additional cyclic carbonate esters, propylene carbonate and vinylene carbonate are extensively used in LIBs. Despite similar chemical structures (Figure 4.1) the SEI derived from EC, PC and VC differ significantly. The following chapters investigate why EC is preferred over PC, the reduction mechanism of EC, and how VC influences SEI formation.

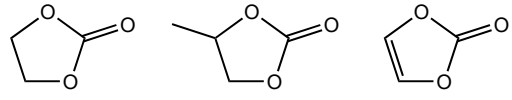

Figure 4.1. The structures of ethylene carbonate, propylene carbonate and vinylene carbonate.

4.1.1 The EC-PC mystery

Propylene carbonate (PC) was initially preferred over EC as an aprotic solvent for Li-metal and Li-ion electrochemistry. The main difference between the properties of PC and EC is the melting point, which enables PC to be used at room temperature. The electrolyte in the first commercial LIB was PC-based. However, with the introduction of graphite as negative electrode, it was quickly realised that PC fails to create a functional SEI while EC succeeds [12]. The disparity in passivation properties between the two solvents is quite surprising since the only difference is a methyl group instead of hydrogen on one of the carbons and this has therefore been subject to numerous studies [65], [66], [67], [68], [69], [70], [71]. Three main theories have been hypothesised explaining the difference in graphite performance in EC- and PC-

derived electrolytes. The first hypothesis assumes that the poor performance stems from severe exfoliation of the graphite structure caused by solvent co-intercalation when using PC-based electrolytes [72]. A second hypothesis is that the two solvents have different reduction pathways, where EC is reduced to a mixture of semicarbonates, polyethylene glycol and $Li_2C_2O_4$, while PC is reduced to Li_2CO_3 [67]. Different SEI compositions would also result in different passivation properties. The most recent hypothesis suggests identical reduction pathways for EC and PC, resulting in lithium ethylene dicarbonate (LEDC) and lithium propylene dicarbonate (LPDC) as shown in Reaction 4.1. The poor passivation is explained by the difference in solubility where LPDC dissolves more readily enabling continuous electrolyte reduction [69].

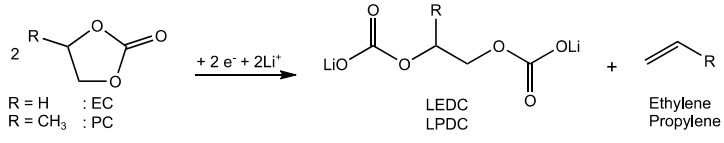

(4.1)

In **Paper I**, the SEI formation in EC- and PC-based electrolytes was investigated with OEMS and EQCM-D. In this study, the most recent hypothesis was supported. Figure 4.2 shows the potential profiles and gas evolution of porous glassy carbon electrodes galvanostatically cycled in 1 M $LiPF_6$ EC:DEC (1:1 volume ratio) and 1 M $LiPF_6$ PC, respectively.

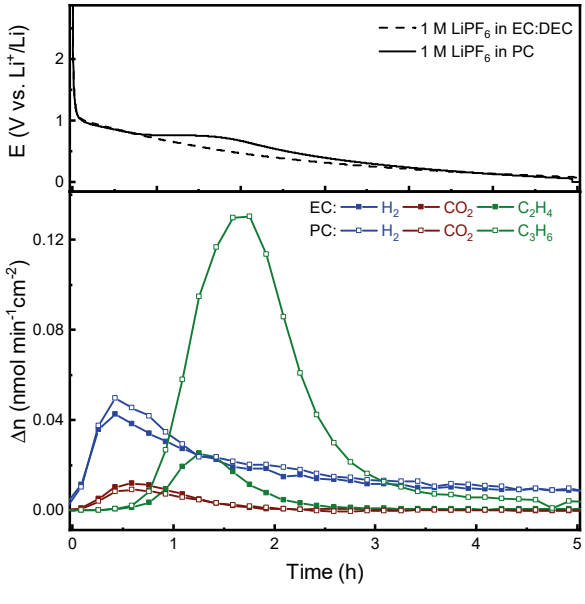

Figure 4.2. Potential profiles, and gas evolution rates of H_2, CO_2, and C_2H_4/C_3H_6 from OEMS measurements of porous glassy carbon electrodes in 1 M $LiPF_6$ in EC:DEC (1:1 volume-ratio) and 1 M $LiPF_6$ in PC during galvanostatic charging at -1 µA cm^{-2}.

Almost instantaneously as the current is applied between the electrodes the potential of the working electrode drops below 1.0V vs. Li^+/Li and H_2 starts evolving regardless of electrolyte. Following the H_2, CO_2 evolution starts. Notably, roughly the same amounts of H_2 and CO_2 evolve in the two electrolytes, indicating identical chain of events. H_2 comes from water and HF reduction, and CO_2 from the OH^--triggered ring-opening reactions of EC and PC. The ring-opening reaction results in alkoxides. The alkoxides continue the ring-opening forming polyethylene glycol and polypropylene glycol according to reaction 4.2.

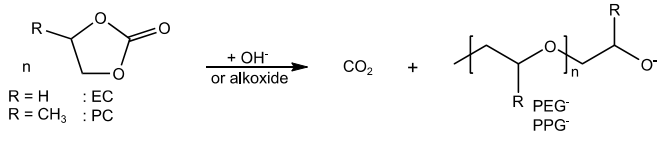

(4.2)

These oligomeric species are formed in the electrolyte and are most likely not confined to the electrode surface and do not contribute to the SEI. As the water is consumed, the potential drops further. At 0.9 V vs. Li^+/Li, ethylene and propylene evolution starts in the EC- and PC-electrolytes, respectively. The potential profile of the electrode in the PC-electrolyte plateaus at 0.9 V vs. Li^+/Li, indicating that a single reduction process can supply enough current to maintain a constant potential while only a small bump is seen in the EC-electrolyte. The alkene evolution correlates well with this trend as one order of magnitude more propylene is evolving (10.1 nmol cm^{-2}) than ethylene (1.4 nmol cm^{-2}). The small amount of ethylene and bump instead of a plateau in the potential points to fast and efficient passivation of the electrode surface as no electrolyte solvent can reach the surface in contrast to the more extensive PC reduction.

The evolution of the mass and the viscoelastic properties of the SEI derived from the PC- and EC-electrolytes are shown in Figure 4.3. As in the OEMS cell, the potential of the carbon EQCM sensor drops fast when current starts flowing. From the open circuit potential (OCP) to 1 V vs. Li^+/Li, the mass deposition is similar in the two electrolytes. In this potential region, HF and water reduction occurs. The expected precipitating products from HF and water are LiF, LiOH and Li_2O, matching the low mpe-values. In this region, the layer deposited on the electrode is thin and rigid, causing a poor fit of the Voigt model. Below 1 V vs. Li^+/Li, the mass deposition rate increases. The increase is significantly smaller in the EC-electrolyte than in the PC-electrolyte, correlating well with the extensive propylene evolution in the OEMS measurement. Looking at the electrolyte viscosity, no major change occurs in the EC-electrolyte while a large increase is observed in the PC-electrolyte simultaneously as the SEI viscosity drops. The decreasing SEI viscosity is explained by the increasing amount of organic species from PC reduction, e.g.

LPDC. A similar trend is observed in the EC-electrolyte, however, much less pronounced.

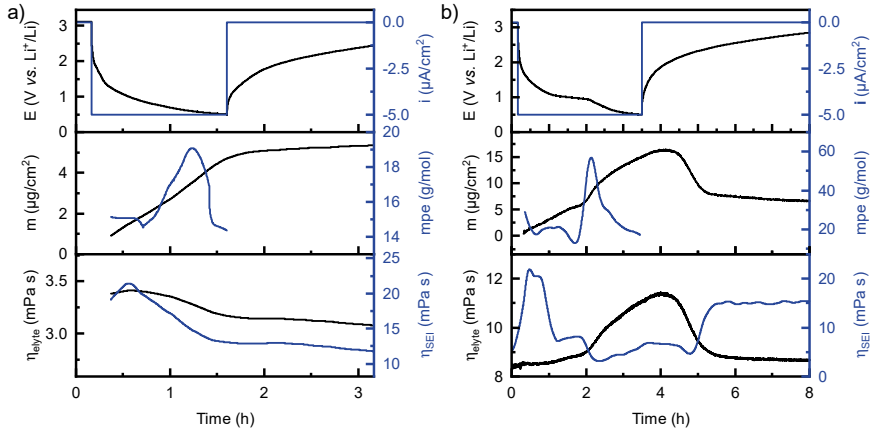

Figure 4.3. Electrode potential of a carbon-coated QCM sensor during the first galvanostatic (−5 µA cm^{-2}) step down to 0.5 V vs. Li$^+$/Li along with the mass and viscoelastic properties of the deposited layers as well as the viscosity of the nearby electrolyte (denoted "elyte") in a) 1 M $LiPF_6$ in ED:DEC (1:1 volume-ratio) and b) 1 M $LiPF_6$ in PC.

After 0.5 V vs. Li$^+$/Li is reached no current or voltage is applied. The layer formed in the EC-electrolyte stops growing and remains stable, while the PC-derived layer remains stable for a short period after which it starts to dissolve. The mass and electrolyte viscosity decrease and the SEI viscosity increases to the same values as at 1 V vs. Li$^+$/Li, meaning that the layer formed during HF and water reduction remains on the electrode surface and the PC-derived species, mainly LPDC, dissolves. The high solubility of LPDC compared to EC-derived SEI species leads to continuous PC reduction during consecutive charge/discharge cycles, unlike the EC-based electrolytes where the electrode surface is mostly passivated during the first charge. This is the main failure mode of graphite electrodes cycled in PC-based electrolytes. The exfoliation of the graphite observed in PC-electrolytes is hence not the cause for the poor performance but rather an effect of the poor passivation.

In addition to the insights into why EC is preferred over PC, the effect of water and $LiPF_6$ on SEI formation is observed. In the EC-electrolyte (Figure 4.3), a substantial amount of mass is deposited before EC reduction (>1 V vs. Li$^+$/Li). This mass deposition stems from HF and water reduction. This thesis aims to study specific passivation processes (e.g. EC reduction) in model systems. Passivation by LiF, LiOH and Li_2O from HF or water reduction might be important process in real application, however, they are problematic in for these model studies since it reduces the amount of the targeted process. This is partially avoided in the following studies by replacing PF_6^- with another anion less prone to hydrolyse, i.e. ClO_4^-.

4.1.2 *Operando* SERS of EC reduction

As demonstrated in **Paper I**, EC undergoes reduction below 0.9 V vs. Li^+/Li. Two main reduction pathways have been suggested. In one pathway two EC molecules are reduced with one electron each creating two EC radicals that combine forming LEDC and ethylene (Reaction 4.2). The other pathway is a direct two-electron reduction of one EC resulting in Li_2CO_3 and ethylene (Reaction 4.3).

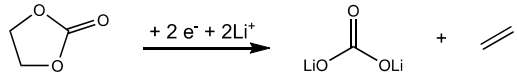

(4.3)

Since ethylene is evolved in Reaction 4.2 and 4.3, determining the predominant pathway with OEMS is impossible. However, the layers formed by LEDC and Li_2CO_3 would have different viscoelastic properties. Theoretically, it should be possible to differentiate between the two with EQCM-D. However, as discussed at the end of the previous section, the EQCM-D measurements are dominated by contaminant reduction processes leaving a small portion of the electrode surface to be passivated by EC reduction. To further investigate the EC reduction, *operando* Raman spectroscopy complemented by OEMS are employed in **Paper II** to study the SEI formation in an electrolyte composed of $LiClO_4$ in EC. For two main reasons, a single-solvent electrolyte was chosen over the typical binary mix of EC and a linear carbonate ester. Firstly, to reduce the number of vibrational bands in the Raman spectra simplifying the spectral analysis. Secondly, the reduction products should be derived from EC. However, the resulting electrolyte has a high viscosity and needs to have a high salt concentration (1.86 M $LiClO_4$) to stay liquid. The high viscosity makes it however non-compatible with EQCM-D.

Figure 4.4 shows the results of *operando* SERS and OEMS measurements of Au working electrodes in $LiClO_4$:EC (1:6 mol-ratio) during the recording of linear sweep voltammogram (LSV) from the OCP to 0.5 V vs Li^+/Li. The dominating bands in the SERS spectrum recorded at the OCP before the polarisation are from free and Li^+-coordinated EC and ClO_4^-. When polarising from the OCP a slight increase of the EC and EC-Li^+ bands is observed as an effect of the electrical double layer (EDL) changing with the electrode potential. At lower potentials, the number of positive charges in the EDL increases to compensate for the build-up of negative charges at the electrode surface. Therefore, a slightly larger increase in the intensity of the EC-Li^+ band is observed. As the electrode potential continues to decrease, faradaic processes start and other species, mostly contaminants, adsorb to the electrode surface pushing free and coordinated EC away from the surface and a decrease of the corresponding bands decrease in intensity.

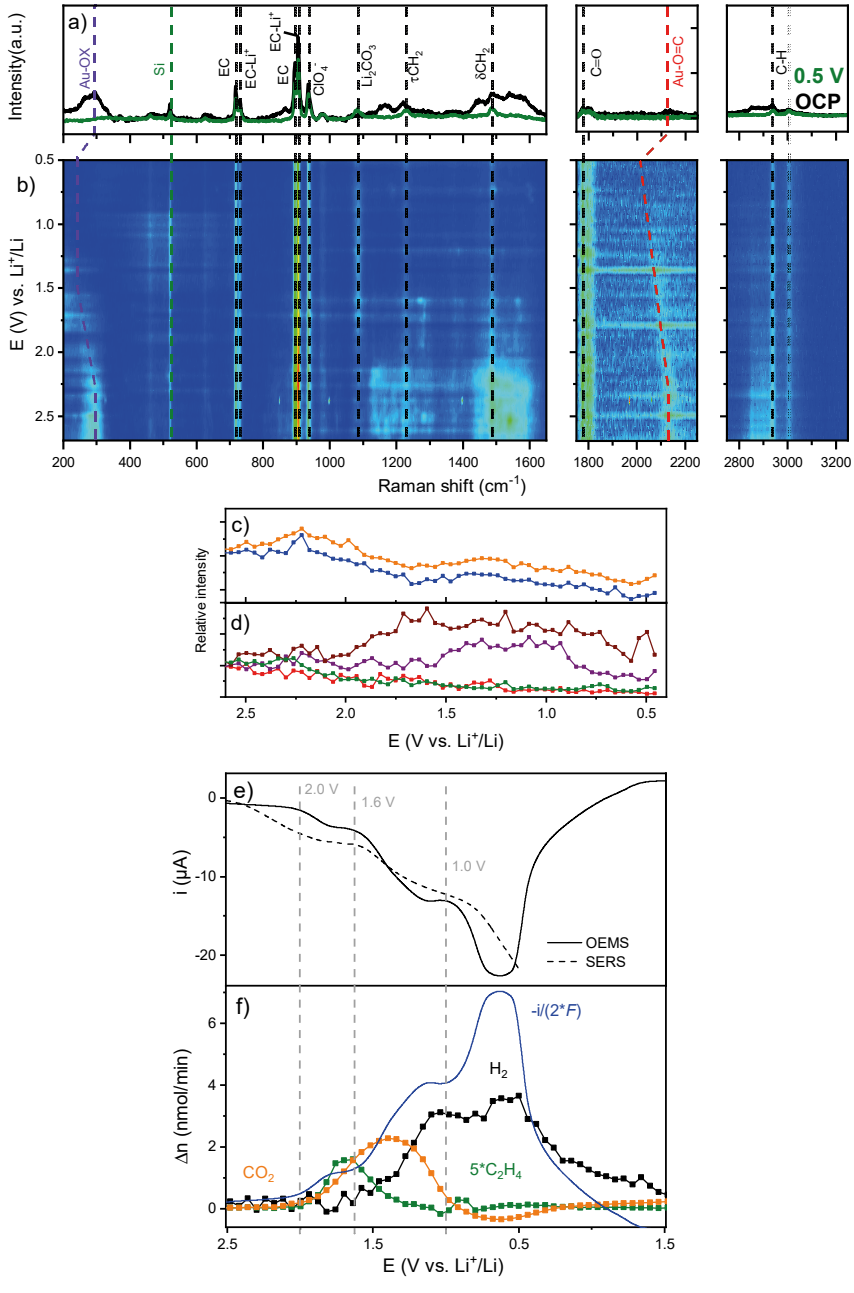

Figure 4.4. a) Raman spectra recorded at the OCP and 0.5 V vs. Li^+/Li, b) *operando* SERS spectra and c) intensities of selected bands relative to those found at the OCP. d) Current recorded in the *operando* SERS cell multiplied by a factor 18 and the OEMS cell. d) The gas evolution rate of H_2, CO_2 and C_2H_4. Linear sweep voltammetry (0.025 mV s^{-1}) of a SERS substrate and cyclic voltammetry (0.1 mV s^{-1}) of an Au-mesh in $LiClO_4$:EC (1:6 mol-ratio) were performed in the SERS and OEMS cells, respectively.

The most unexpected finding in this study is that as the Au electrodes are polarised to below 2.0 V vs. Li^+/Li, a band at 1085 cm^{-1} assigned to Li_2CO_3 emerges in the SERS spectra and ethylene evolution starts in the OEMS cell. No other processes besides EC reduction are likely to result in Li_2CO_3 and ethylene in this system. However, a shift from 0.8 to ~2.0 V vs Li^+/Li is too large to be explained by the catalytic effects of Au. The total amount of ethylene evolved is roughly 4 nmol cm^{-2} and assuming one ethylene per Li_2CO_3 this is equivalent to a 1.4 nm thick Li_2CO_3. No emerging vibrational bands could be assigned to LEDC, indicating that the reduction pathway shown in Reaction 4.2 is not favoured at Au electrodes. Compared to the ethylene evolution relative to H_2 and CO_2 on carbon in **Paper I**, it is clear that the EC reduction process on Au is less pronounced, and the reduction of contaminants dominates. Converting the current recorded in the OEMS cell into a gas evolution rate, assuming a two-electron process per gas molecule, it is clear that most of the current goes to water reduction where two electrons yield one H_2.

Additional peaks at 292 and 2133 cm^{-1} in the OCP spectrum are assigned to O_x and O=CR type species absorbed on the Au surface. Prior to the formation of Li_2CO_3 and ethylene evolution, as the Au SERS substrate is polarised from the OCP to 2.0 V, the bands assigned O_x and O=CR surface species shift to lower wavenumbers suggesting chemisorbed species on the Au surface due to the Stark effect [73]. However, the shift is significantly larger than expected as the Stark effect often results in one-fourth of the observed shift. The bands do not only shift but also decrease in intensity as the surface groups are reduced. Simultaneously as these oxygen-containing species are reduced, two bands appear at 523 and 1140 cm^{-1} which can be assigned to Li_2O and superoxide. Similar to OH^-, superoxide reacts with and ring-open EC leading to PEG^- and CO_2. This agrees well with the CO_2 evolution starting before water reduction.

At 1.6 V, water reduction starts and H_2 and OH^- are produced leading to ring-opening of EC and CO_2 evolution. As the H_2 evolution increases, the CO_2 evolution rate starts to decrease due to the equilibrium between OH^-, CO_2 and bicarbonate (Reaction 4.4). Below 1.0 V vs. Li^+/Li, the evolution rate of CO_2 is negative, meaning that CO_2 is consumed. Two reduction pathways of CO_2 are expected where one is a reduction of the bicarbonate leading to Li_2CO_3 and H_2 (Reaction 4.5). The other pathway is a direct reduction leading to $Li_2C_2O_4$ (Reaction 4.6).

$$CO_2 + OH^- \rightleftharpoons HCO_3^- \tag{4.4}$$

$$HCO_3^- + 2Li^+ + e^- \rightarrow Li_2CO_3 + \frac{1}{2} H_2 \tag{4.5}$$

$$2CO_2 + 2Li^+ + 2e^- \rightarrow Li_2C_2O_4 \tag{4.6}$$

Formation of $Li_2C_2O_4$ could explain the deviation between the current converted into gas evolution rate and the sum of the gas evolutions as no gas is evolved in this pathway. However, no spectroscopic evidence of $Li_2C_2O_4$ is found in the SERS spectra. A slight increase in the H_2 evolution rate is observed at 0.75 V vs. Li^+/Li. This increase is consistent with the reduction of bicarbonate. As the SEI grows and covers more of the Au surface, it becomes less reflective. This reduction in reflectivity reduces the surface enhancement effect, decreasing all vibrational bands in the SERS spectra.

The exclusion of PF_6^- (and its derivatives) from the system simplifies the SEI formation and enables further insights regarding the reduction of EC to be obtained. Still, the effects of contaminants (mainly water) are obvious in **Paper II**. Even though the electrolyte is prepared with pure and dry chemicals, ppm-level contaminants are enough to dominate the initial SEI formation process, especially in systems with high flooding factors. Getting rid of ppm-amounts of contaminants is notoriously difficult and not viable from a commercial point of view. Hence the effect of these on the SEI formation is still important to study and understand, even if the effect is much smaller in commercial cells compared to the model systems used herein. Another aspect to consider is the effect of the working electrode on SEI formation. In **Paper I**, ethylene evolves around 0.8 V vs. Li^+/Li at carbon whereas in **Paper II** it evolves close to 2.0 V vs. Li^+/Li at Au.

4.1.3 EQCM-D of the effect of VC

At the end of the 1990s, VC, the archetypical LIB electrolyte additive, was introduced and initially explored as an electrolyte solvent for LIBs [74]. Later studies found VC to be more effective as an electrolyte additive and showed that small amounts of VC improved the capacity retention, cycle life, and decreased the SEI thickness of graphite electrodes [75], [76], [77], [78]. The reduction potential of VC is claimed to be higher than those of the other electrolyte components (>1.0 V vs. Li^+/Li) where cleavage of the bond between oxygen and vinylic carbon causes a ring-opening according to Reaction 4.7. The resulting radical is highly reactive and numerous reaction pathways have been proposed with dimers and oligomers such as lithium di-vinylene di-carbonate (LDVD) and poly(VC) as products [78], [79], [80]. More recent studies have shown increased CO_2 evolution at potentials higher than where VC is expected to be reduced. The CO_2 evolution is claimed to stem from ring-opening reactions induced by reduced oxygen species and OH^- from water reduction. The ring-opened VC radical starts a polymerisation of VC (and EC) releasing CO_2 [81], [82]. The common feature of the final product in all proposed reaction pathways are unsaturated bonds. These have been shown by Gogoi et al. to act as water scavengers [83].

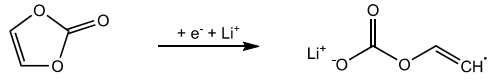

(4.7)

In **Paper III**, the effect of VC addition to 0.2 M $LiClO_4$ EC:DEC (1:9 volume ratio) was investigated by EQCM-D coupled with electrochemical impedance spectroscopy (EIS). Figure 4.5 presents the chronoamperometric, EQCM-D and EIS results of the Au QCM-sensor in the electrolyte mentioned above with and without VC. Chronoamperometric measurements were performed by stepping the potential of the Au QCM sensor electrodes from 2.0 to 0.6 V vs. Li^+/Li with increments of 0.2 V. The Li^+ transport properties of the layers formed were investigated by EIS after each potential step. Below 2.0 V vs. Li^+/Li, numerous faradaic reactions occur which would affect the EIS spectra, making the interpretation and extraction of SEI properties challenging. Therefore, before each EIS measurement, the potential was held at 2.0 V vs. Li^+/Li for 1 h after which EIS spectra were recorded. At 2.0 V vs. Li^+/Li, no faradaic processes are expected to occur except during the first step from the OCP to 2.0 V vs. Li^+/Li where oxygen contaminants are reduced and consumed. Consequently, the EIS spectra are recorded under blocking conditions, without contribution from charge transfer resistance. In addition, the mass and dissipation change at 2.0 V vs. Li^+/Li would reveal any chemical reactions with precipitating products that are initiated at the lower potentials while the current can be used to identify the oxidation of the interphase species. During the potential steps there is underpotential deposition (UPD) of Li on the Au electrode. Early EQCM work on similar electrolytes by Zaban and Aurbach noted that a low mpe-value around 7 g mol^{-1} at low potentials is an indication of UPD and a well-functioning passivation layer [47]. A later study by Mo et al. showed that roughly 100 ng cm^{-2} can be accounted for mainly by UPD between 2.0 and 0.6 V vs. Li^+/Li [84].

From 2.0 to 1.4 V vs. Li^+/Li, the consumed charge, mass and dissipation were virtually identical in all electrolytes. Even though no significant change in the interphase can be detected via EQCM-D or chronoamperometry, higher SEI resistance is observed in the VC-electrolytes. As the resistance is inversely proportional to Li^+ concentration easily accessible to the electrode, the higher resistance indicates lower Li^+ concentration in the VC-derived interphase. This could indicate the formation of an island-like structure of SEI species hindering Li^+ from the electrolyte to access the electrode in contrast to the EC-electrolyte where the electrode surface is clear from SEI products. At 1.4 to 1.0 V vs. Li^+/Li, a larger increase in charge, mass and dissipation is observed in the EC-electrolyte compared to the VC-electrolytes in which only subtle increases are observed. The SEI resistance drops for the VC-electrolytes while it remains unchanged in the EC-electrolyte. EC reduction is not expected above 1.0 V vs. Li^+/Li, and the current is dominated by mainly water reduction leading to OH^- confirmed by complementary OEMS measurements

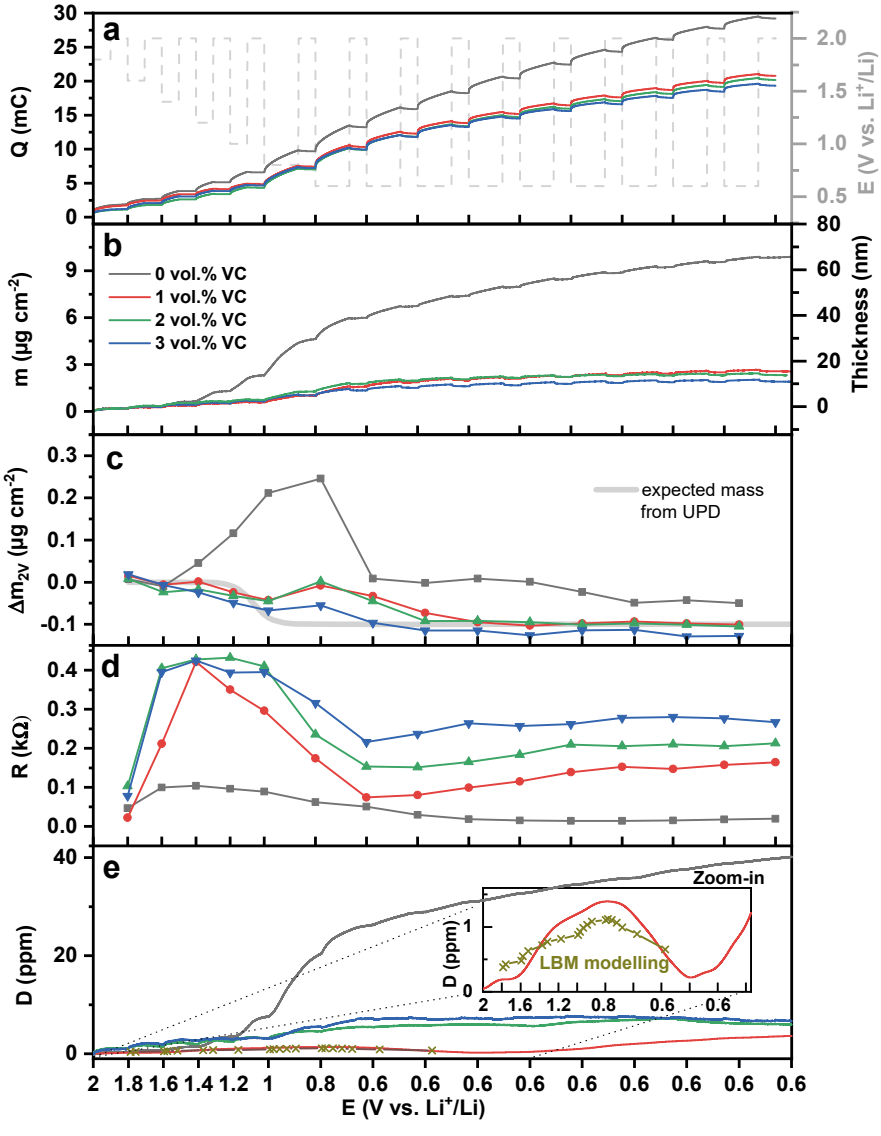

Figure 4.5. a) The accumulative charge and electrode potential, b) the mass and thickness of the layer deposited on the QCM sensor, c) the mass change during the potential steps to 2.0 V vs. Li^+/Li and the corresponding underpotential deposition coverage adapted from [84], d) the fitted SEI resistance from the EIS measurements at 2.0 V vs. Li^+/Li and d) the dissipation of an Au electrode in 0.5 M $LiClO_4$ EC:DEC (1:9 volume-ratio) with 0, 1, 2 and 3 vol.% VC. The inset in e) shows the dissipation of the layer formed with 1 vol.% VC and the dissipation from Frequency Domain Lattice Boltzmann Method (FD-LBM) modelling of homogenous nucleation (at 2.0 V vs. Li^+/Li) and growth of a layer reaching solidification at the third potential step at 0.6 V vs. Li^+/Li.

(shown in **Paper III**), in agreement with **Papers I** and **II**. OH^- will produce PEG^- by ring-opening of EC. An alternative reaction pathway between OH^- and EC have previously been proposed leading to lithium ethylene monocarbonate (LEMC) [85] which is in equilibrium with LEDC and ethylene glycol according to Reaction 4.8 and 4.9 [86]. An alternative route to LEDC is a reaction between an OH^- ring-opened EC and CO_2. LEDC and LEMC are common SEI species and are often regarded to be important for passivating the electrode. However, that is not the case in these measurements as the mass and dissipation continue to increase. These chemical reactions are seen in the mass change during the potential steps at 2.0 V vs. Li^+/Li where the mass increases despite the absence of electrochemical reactions.

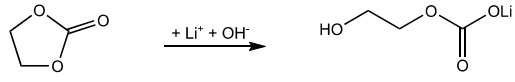

(4.8)

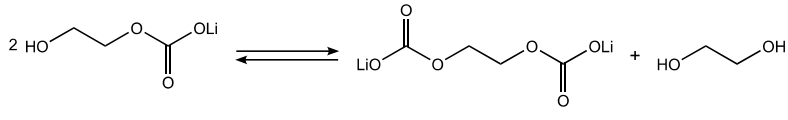

(4.9)

Below 1.0 V vs. Li^+/Li, EC reduction is expected, however, no ethylene evolution is observed. The layer formed in the EC-electrolyte continues to follow the same trends with increasing mass and dissipation without any change in the SEI resistance. A sharp decrease in the mass change at 2.0 V vs. Li^+/Li is observed between the 1.0 and 0.8 V vs. Li^+/Li steps. This indicates that the chemical reactions, mainly driven by OH^-, stop. Below 1.0 V vs. Li^+/Li, both EC and CO_2 reduction are expected and seem to form a layer that suppresses water reduction. After 8 potential steps to 0.6 V vs. Li^+/Li, the EC-derived layer has a mass of 10 µg cm^{-2}. Assuming the layer is homogenous and dense with a density of 1.4 g cm^{-3}, the mass would correspond to a 70 nm thick layer. This should be more than enough to passivate and increase the SEI resistance. Counterintuitively, the SEI resistance decreases slightly from 1.4 V vs. Li^+/Li while the layer grows. This points to the formation of a highly porous layer that does not hinder the electrolyte from coming in contact with the electrode as the resistance.

In the VC-electrolytes below 1.2 V vs. Li^+/Li, the mass deposition rate slightly increases. The increase is attributed to VC and CO_2 reduction leading to formation of Li_2CO_3 and $Li_2C_2O_4$. In the 1 vol.% VC electrolyte, the dissipation increases with the mass until the first potential step at 0.6 V vs. Li^+/Li. During the three subsequent potential steps, the dissipation approaches 0 ppm. A decrease in dissipation indicates that the layer becomes more rigid, as expected for an island-like film reaching percolation and solidification. This

suggests that the VC-derived SEI becomes less porous. To investigate this theory further, Frequency Domain Lattice Boltzmann Method (FD-LBM) is employed to model such a growth process. The FD-LDM model results, as shown in the inset of Figure 4.5 e), are consistent with the experimental data. Notably, a consistent mass decrease of 100 ng cm^{-2} is observed at 2.0 V vs. Li^+/Li between the repeated steps to 0.6 V vs. Li^+/Li. This mass change is not attributed to the dissolution of the SEI but rather, to the UPD of Li on Au in agreement with [84] and is a clear indication of a functioning passivation layer.

The cumulative charge, mass and gas evolution for the EC-electrolyte is higher than in the VC-electrolytes. High dissipation and low resistance indicate that the EC-derived layer is highly porous. As the current is dominated by water reduction and no ethylene evolution is detected, the layer is formed by hydrolysis and OH^--induced ring-opening of EC. Conversely, the VC-derived SEI, despite being significantly thinner, passivates the electrodes effectively. The layer hinders reduction of contaminants and electrolyte solvents to a greater extent than the EC-derived layer. Notably, while EC and water concentrations are equal in all electrolytes, the addition of a small amount of VC to the electrolyte significantly improves passivation without developing a thick EC-derived layer. The exact mechanism behind this is not fully understood. However, based on the findings herein, it is hypothesised that the combination of OH^--initiated chemical reactions and electrochemical reduction of VC, and its derivatives (e.g. CO_2), forms a thin rigid SEI. As in **Papers I** and **II**, the SEI formation is dominated by reduction of contaminants (mainly H_2O) in **Paper III**. Avoiding contaminants is challenging, especially since all components in a LIB are hygroscopic. This study shows the effective passivation process of VC in the presence of H_2O impurities and elucidates the importance and crucial role VC has as an electrolyte additive in LIBs.

In **Papers II** and **III** Au electrodes are utilised to investigate SEI formation. Au has different electrocatalytic properties compared to carbon/graphite electrodes found in real LIBs, which could potentially alter the reduction pathways of EC and VC. In paper II ethylene evolution is detected more than 1 V higher than expected on carbon. However, when comparing the findings in **Paper III** to the literature many similarities are found. In the VC-electrolytes, the onset potential of the main formation process of a well-functioning SEI occurs at <1.4 V vs. Li^+/Li as the SEI resistance decreases and the mass increases, reaching stable resistance and mass around 0.6 V vs. Li^+/Li. A similar trend and final SEI resistance is observed in the EIS study by Solchenbach et al. on graphite electrodes in VC-containing electrolytes [87]. Additionally, previous studies have reported a significant reduction in SEI thickness when incorporating VC in the electrolyte [49], [88].

4.2 Alternative layer-forming additives

Tailoring the formation and properties of electrode-electrolyte interphases is crucial for improving the performance of current LIBs chemistries and enabling new chemistries (e.g. high potential cathodes, Si or Li-metal electrodes). Incorporating moieties into the SEI with a central atom other than C or O can significantly alter its properties, including physical and chemical stability and Li^+-ion conductivity. Incorporation of such moieties is typically achieved through the addition of electrolyte additives [89]. While additives are used extensively to optimise performance, studies of the underlying reaction pathways are often overlooked. To deepen the fundamental understanding of the reduction mechanism of one B-based (LiBOB) and two S-based (DTD and PES) layer-forming additives are investigated in **Paper IV** and **V**, respectively.

These additives are studied in a model system comprised of a porous glassy carbon (GC) working electrode voltammetrically cycled in 0.2 M $LiClO_4$ dissolved in DME (referred to as the Baseline electrolyte). Using GC as a model electrode over Au is motivated by its conceivably similar surface structure to graphite, yet effects associated with solvent co-intercalation can be avoided. In addition, Au and S are known to interact strongly, which could further complicate or alter the reduction mechanisms of S-based additives. Furthermore, to enable clear detection of species with OEMS and *operando* FTIR, a high electrode surface area (and amount of SEI compounds) is needed. This is much easier to achieve with GC than with Au. $LiClO_4$ in DME is chosen as the model electrolyte due to its low reduction potential and the commercial availability of high purity.

4.2.1 Reduction mechanism of LiBOB

LiBOB was introduced as an alternative electrolyte salt for LIBs in 1999 [90]. Subsequent studies found LiBOB to function not only as an electrolyte salt but also as a layer-forming additive creating passivation layers on both the negative and positive electrodes [91], [92], [93]. On the negative electrode, LiBOB is reported to form an SEI as it is reduced at approximately 1.8 V vs. Li^+/Li. As previously mentioned, water reduction occurs at 1.6 V vs. Li^+/Li and leads to numerous unwanted chemical reactions between OH^- and electrolyte salt and solvents. Therefore, LiBOB is unique among layer-forming additives as most form an SEI at potentials lower than water reduction. Several reduction mechanisms for LiBOB have been proposed. In **Paper IV**, the reduction pathway and the passivation properties of LiBOB-derived SEI are studied with *operando* ATR-FTIR, OEMS and EQCM.

Figure 4.6 shows the *operando* ATR-FTIR measurement of a GC electrode during a LSV scan from the OCP to 0.5 V vs. Li^+/Li in 0.2 M $LiClO_4$ DME + 50 mM LiBOB. The *operando* absorbance spectra remain unchanged from the

OCP to 1.8 V vs. Li^+/Li. At this potential, a reductive current starts flowing and the vibrational bands at 1807 and 1780 cm^{-1} attributed to vibrational modes of the carbonyl group of BOB^- decrease in intensity indicating BOB^--consumption. Simultaneously, three positive bands appear at 1664, 1326 and 782 cm^{-1} assigned to $Li_2C_2O_4$. The BOB^- bands follow the current and around 1.5 V vs. Li^+/Li, the current starts to decay and the band intensity increases as the local interfacial BOB^- concentration is restored to the bulk electrolyte concentration. The $Li_2C_2O_4$ bands stop growing and remain at a constant intensity.

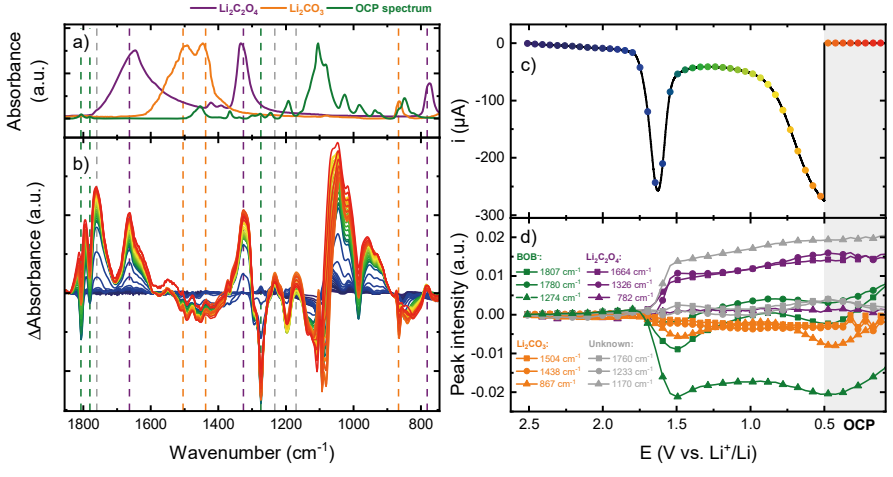

Figure 4.6. a) Reference spectra of 0.2 M $LiClO_4$ in DME + 50 mM LiBOB, $Li_2C_2O_4$ and Li_2CO_3. b) *Operando* ATR-FTIR absorbance spectra (relative to the OCP spectrum) of a porous glassy carbon electrode during linear sweep voltammetry from the OCP to 0.5 V vs. Li^+/Li in the LiBOB electrolyte mentioned above, c) the current response and d) intensities of selected vibrational bands.

The negative band at 1274 cm^{-1} is not discussed in **Paper IV** due to the overlap with DME rendering the assignment uncertain. However, this band is commonly assigned to a bending mode of O-B-O of BOB^- [94], [95]. It starts decreasing at 1.8 V vs. Li^+/Li in the *operando* spectra and follows the same intensity profile as the carbonyl bands of BOB^-. According to Reaction 4.10, these bonds break when BOB^- undergoes reduction resulting in $Li_2C_2O_4$.

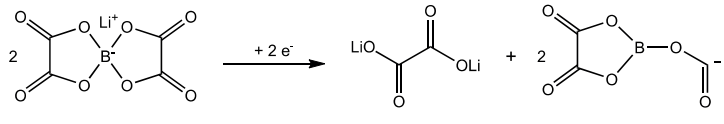

(4.10)

Voltammograms recorded in the EQCM and OEMS cells using the Baseline electrolyte with and without LiBOB and EC are shown in Figure 4.7. The voltammograms of the LiBOB-containing electrolytes are similar to the ATR-

FTIR cell with a clear reduction peak at 1.8 V vs. Li^+/Li assigned to BOB^- reduction. No significant current or mass deposition in the EQCM cell is recorded for the Baseline electrolyte, confirming the cathodic stability of the formulation. A slight increase in mass is seen below 1.0 V vs. Li^+/Li where the Li^+ adsorption capacity increases. In the LiBOB-electrolyte, mass deposition starts and follows the charge consumed by BOB^- reduction. At the peaks in the voltammogram around 1.6 V vs. Li^+/Li, a mpe-value of roughly 50 g mol^{-1} is observed which matches well with a two-electron per $Li_2C_2O_4$ process. After reaching 0.5 V vs. Li^+/Li, the sweep direction changes and the layer deposited on the sensor remains stable at 2.5 µg cm^{-2}, showing no tendencies of dissolution. Assuming this is a dense $Li_2C_2O_4$ layer, the thickness is 12 nm.

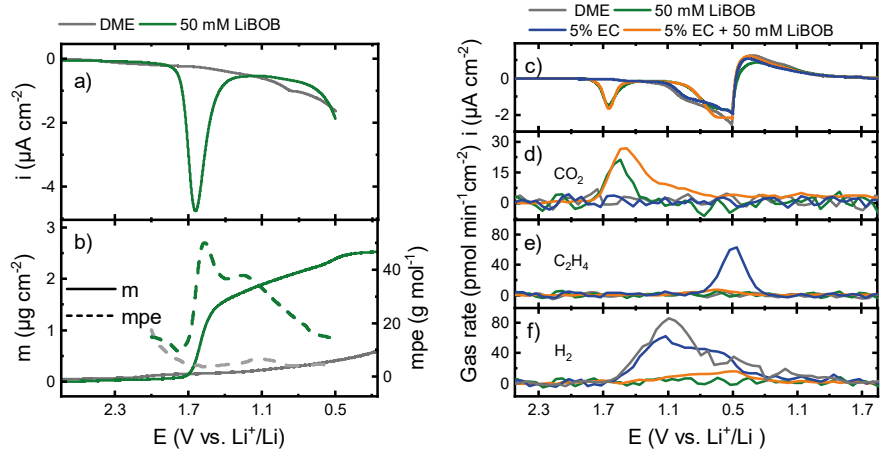

Figure 4.7. Voltammograms of carbon electrodes recorded in the a) EQCM and c) OEMS cell in 0.2 M $LiClO_4$ DME with and without LiBOB and EC. b) The mass deposition and mass per electron (mpe) value on the carbon QCM sensor and d-e) the gas evolution rates of CO_2, C_2H_4 and H_2.

To examine the passivation properties of the layer formed by BOB^- reduction, two additional electrolytes were investigated with OEMS. One with 5 vol.% EC (EC-electrolyte) and one with 5 vol.% EC + 50 mM LiBOB (EC+LiBOB). In both LiBOB-containing electrolytes, the peak at 1.8 V vs. Li^+/Li in the voltammogram is accompanied by CO_2 evolution, indicating an additional reduction pathway of BOB^- as no CO_2 is expected according to Reaction 4.10. Therefore, an alternative reduction pathway where CO_2 evolves is suggested according to Reaction 4.11. However, the amount of CO_2 evolved in the LiBOB-electrolyte (0.85 nmol cm^{-2}) is significantly lower than the charge consumed during the BOB^- reduction (24.3 nmol electrons cm^{-2}), hence CO_2 formation is a minor part of a major reaction pathway. The CO_2 evolution follows the current profile in the LiBOB-electrolyte while in the EC+LiBOB the CO_2 evolution continues below 1.5 V vs. Li^+/Li even though no reductive current flows through the cell. This CO_2 tail indicates a chemical step following the

electrochemical reduction of BOB^- reaction. A possible chemical step is presented in Reaction 4.12. Notably, the reactant in this reaction is a product in both Reaction 4.10 and 4.11. Hence, it is difficult to determine the exact reaction pathway for CO_2 evolution as it could be from direct electrochemical reduction of BOB^- together with a subsequent chemical step.

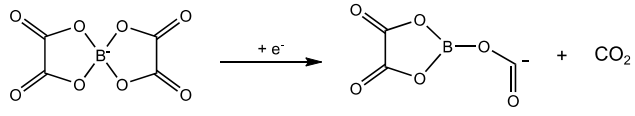

(4.11)

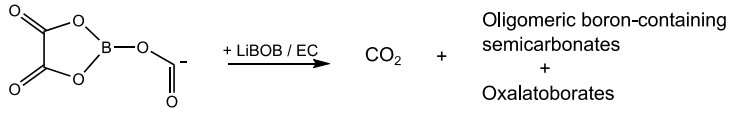

(4.12)

At 1.6 V vs. Li^+/Li water reduction is observed as a current plateau and H_2 evolution in the DME- and EC-electrolyte. In the LiBOB-electrolytes, no H_2 is evolved. Below 0.8 V vs. Li^+/Li, ethylene is evolved from the EC reduction in the EC-electrolyte. No ethylene is evolved when LiBOB is present with EC in the electrolyte. This indicates that the LiBOB-derived layer sufficiently passivates the electrode hindering water and EC from being reduced. As shown in **Papers I**, **II** and **III**, water reduction greatly impacts the SEI formation and its composition which in turn affects the performance of a LIB. The improved performance and cycle life observed when LiBOB is incorporated as an electrolyte additive is likely partly explained by the effective suppression of water reduction.

4.2.2 Reduction mechanism of DTD and PES

Two of the most prominent sulphur-based layer-forming additives are 1,3,2-dioxathiolane 2,2-dioxide (DTD) and prop-1-ene-1,3-sultone (PES). DTD has a structure similar to EC but with a sulphate group instead of a carbonyl group. PES displays a similar structure to DTD, but one oxygen in the ring is replaced with a carbon with an unsaturated bond. Both additives have been shown to improve the performance of LIBs significantly [96], [97]. Multiple reaction pathways for DTD and PES with various $ROSO_2Li/ROSO_3Li$ species, Li_2SO_3 and Li_2SO_4 have been proposed. In **Paper V**, DTD and PES are studied in a model system (same as in **Paper IV**) with various *operando* techniques to assess and sort out the most accurate reduction pathways.

Figure 4.8 shows cyclic voltammograms of GC electrodes in 0.2 M $LiClO_4$ DME with and without DTD, EC and DTD+EC along the *operando* ATR-FTIR, OEMS and EQCM measurements. The first electrochemical process occurs at 2.4 V vs. Li^+/Li in the DTD-electrolytes where a small reductive peak appears. Two possible explanations for this high-potential process are

hypothesised. One is reduction of a contaminating residue from the DTD synthesis. The other explanation is a combined reduction and ring-opening of DTD, as suggested by Jankowski et al. [98]. This reduction is not accompanied by any significant gas evolution or change in the intensity of the vibrational band at 1388 cm^{-1} (assigned to DTD), but mass deposition on the carbon QCM sensors. The mass increases independent of current and continues to increase until 6 μg cm^{-2} for both DTD-electrolytes, indicative of a chemical reaction initiated by the electrochemical reaction at 2.4 V vs. Li^+/Li. When EC is present, the mass deposition reaches passivation above 1.0 V vs. Li^+/Li while the mass deposition rate is slightly lower in the DTD-electrolyte without EC reaching passivation at the end of the negative potential sweep. Below 1.6 V vs. Li^+/Li, H_2 evolution starts in all electrolytes. Compared to the baseline electrolyte (with in total 0.7 μmol H_2), twice the amount of H_2 evolved in the DTD-electrolytes (1.4 μmol H_2), largely in agreement with the observed currents around this potential. This increased H_2 evolution is believed to stem from water contamination of the DTD as it is difficult to dry due to its thermal instability.

Water reduction is followed by a second reduction process at 1.4 V vs. Li^+/Li in the DTD-electrolytes. This latter process is attributed to the main reduction process of DTD as evidenced by a concurrent decrease of the vibrational band at 1388 cm^{-1} and ethylene evolution. The charge consumed by this reaction in the DTD-electrolytes (12 nmol cm^{-2}) is more than two times larger than the total ethylene evolution (4.7 nmol cm^{-2}) which implies a reaction pathway where more than one electron per ethylene is consumed. A two-electron reduction is not unlikely as it overlaps with water reduction which will consume additional of the charge resulting in ratio slightly between charge and ethylene higher than two. Among previously proposed reduction pathways of DTD, two are more likely as two electrons are consumed and ethylene forms, according to Reaction 4.13 and 4.14. Simultaneously as DTD is reduced, a slight decrease in the vibrational band attributed to EC in the DTD+EC electrolyte can be seen. This indicates a chemical reaction between reduced DTD and EC.

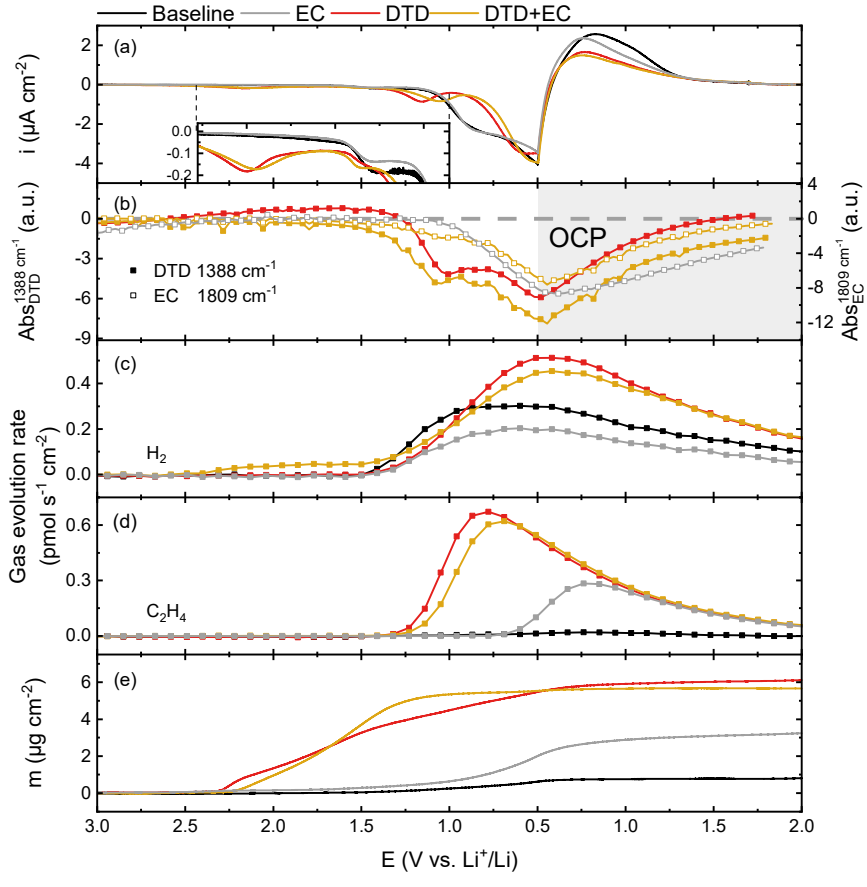

Figure 4.8. a) Cyclic voltammograms of glassy carbon electrodes cycled in 0.2 M $LiClO_4$ DME and with the addition of 5 wt.% EC, DTD, and a combination of both with corresponding b) peak intensity change of the main vibration bands of DTD and EC (1388 and 1809 cm^{-1}) from *operando* ATR-FTIR, gas evolution rate of c) H_2 and d) C_2H_4 from OEMS and e) electrode mass change from EQCM-D. The absorbance values are relative to the spectra taken after 7500 s, where the baseline drift stabilises.

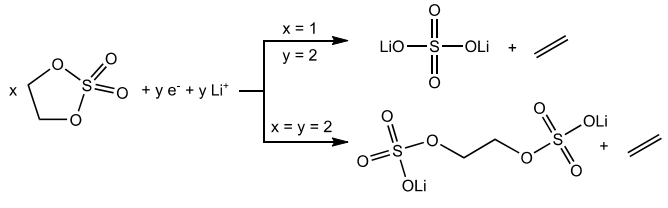

(4.13)

(4.14)

The ethylene evolution continues long after the reduction starting at 1.4 V vs. Li^+/Li is over, indicating an intermediate step between the reduction and ethylene evolution, in line with previously suggested reduction pathways [99]. An intermediate step would explain the continuous ethylene evolution well

after the reduction is over. Similarly, an intermediate step in Reaction 4.14 is required. Two DTD molecules are reduced by one electron each to DTD radicals. These radicals could also survive in the electrolyte before combing into lithium ethylene disulfate and ethylene. Below 0.8 V vs. Li^+/Li, EC reduction is expected and seen in the EC-electrolyte as the intensity of the vibrational band assigned to EC decreases ethylene evolution and mass deposition occurs. In the DTD-electrolyte EC reduction is suppressed as no additional ethylene evolution peaks or mass increases are observed. Despite this observation, in the DTD+EC-electrolyte the EC vibrational band decreases from 0.8 to 0.5 V vs. Li^+/Li, indicating EC consumption. When 0.5 V vs. Li^+/Li is reached, a positive sweep is performed except for in the *operando* ATR-FTIR cell which is let to equilibrate at OCP. During the positive potential sweep, no dissolution or additional gas evolution occurs. At the OCP, the vibrational bands for EC and DTD slowly increase as the concentration of EC and DTD in the probed volume equilibrates with the bulk electrolyte.

Figure 4.9 shows measurements analogous to those in Figure 4.8, but for PES instead of DTD. No activity in the voltammograms, absorbance spectra, gas evolution or EQCM measurement is observed until water reduction onsets. In contrast to the DTD-electrolyte, the H_2 evolution in the PES-electrolyte is significantly lower (0.4 µmol) compared to the baseline electrolyte (0.7 µmol) despite the current being twice as high for the PES-electrolyte at 1.6 V vs. Li^+/Li. As for DTD, the water reduction is followed by a reduction starting at 1.4 V vs. Li^+/Li. Simultaneously with this reduction, the vibrational band at 1344 cm^{-1} assigned to PES decreases in intensity as evidence for PES reduction. In the PES+EC-electrolyte, the EC vibrational band decreases significantly as PES is reduced, indicating that reduced PES is even more reactive towards EC compared to reduced DTD. As soon as the PES reduction starts, the H_2 evolution plateaus and remains constant throughout the voltammogram. This indicated that reduced PES species, e.g. Li_2PES, are prone to abstract reduced protons from the electrode surface before they can combine to H_2, in agreement with DFT calculation performed by Self et al. showcasing this proton abstraction to be highly exergonic [100]. According to their calculations, Li_2PES can abstract two protons, forming Li_2SO_3 and propylene (shown in Reaction 4.15). However, no additional gas evolution is observed but a mass deposition process is initiated in the PES-electrolytes. When comparing the charge consumed during the PES reduction (23 nmol cm^{-2} in the PES-electrolyte) with the difference in H_2 evolution relative to the baseline electrolyte (1.5 and 3.5 nmol cm^{-2} in the PES electrolyte and Baseline, respectively), it is obvious that only a small portion of the reduced PES is taking up a hydrogen radical which could explain the absence of propene in the OEMS measurement.

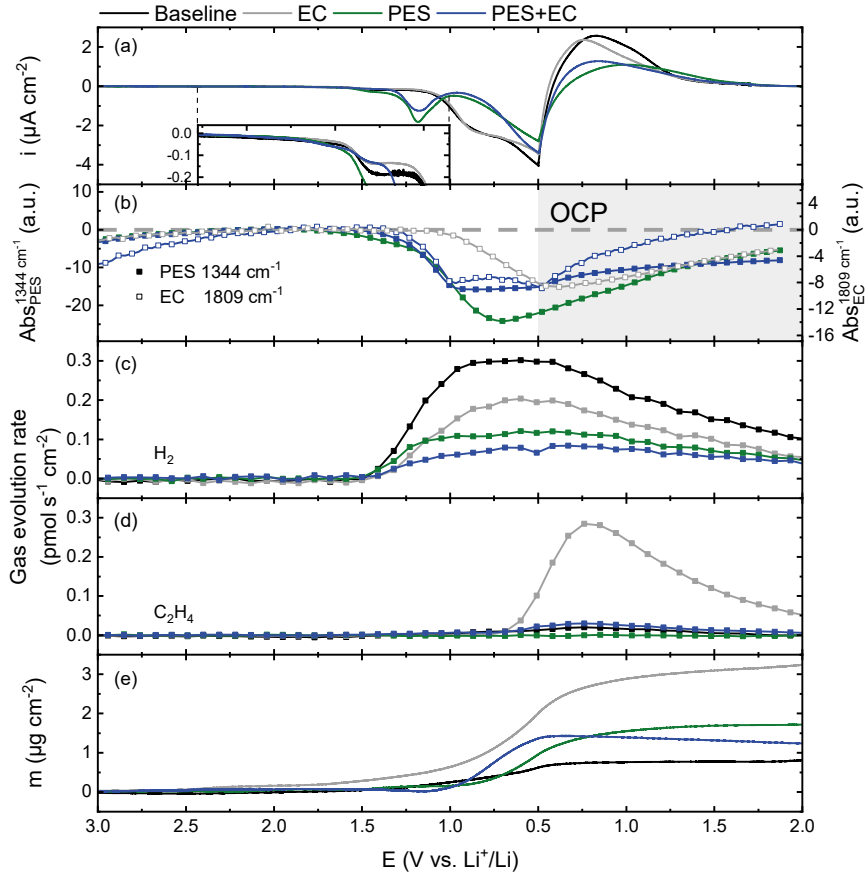

Figure 4.9. a) Cyclic voltammograms of glassy carbon electrodes cycled in 0.2 M $LiClO_4$ DME and with the addition of 5 wt.% EC, PES, and a combination of both with corresponding b) peak intensity change of the main vibration bands of PES and EC (1344 and 1809 cm^{-1}) from *operando* ATR-FTIR, gas evolution rate of c) H_2 and d) C_2H_4 from OEMS and e) electrode mass change from EQCM-D. The absorbance values are relative to the spectra taken after 7500 s, where the baseline drift stabilises.

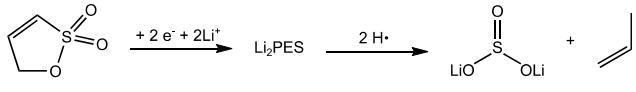

(4.15)

The major mass deposition onset is slightly lower in potential, ~1.0 V vs. Li^+/Li, than the observed reduction in the voltammogram. However, a slightly negative mass is recorded around 1.4 V vs. Li^+/Li when PES is present. This could be an indication of gas evolution or a decrease in electrolyte viscosity close to the electrode. Since no gas is observed, a decrease in electrolyte viscosity is more likely. This in combination with the shift in mass deposition could be explained as a chemical step proceeding with the PES reduction,

eventually leading to solid products depositing on the electrode surface. Comparing the mass deposition in the two PES-electrolytes, passivation is reached faster when EC is present and shows a slight dissolution during the positive sweep while in the pure PES-electrolyte mass continues to increase during the positive sweep until 1.0 V vs. Li^+/Li (still below the reduction potential of PES).

In contrast to the *operando* ATR-FTIR measurements of the Baseline, EC-, DTD- and DTD+EC-electrolyte, new vibrational bands emerge in the PES-electrolytes as PES is being reduced. Figure 4.10 shows the *operando* absorbance spectra of porous GC electrodes polarised in the PES- and PES+EC-electrolytes along the current response and intensities of selected vibrational bands. The band at 1344 cm^{-1} is assigned to PES evidenced by the peak in the difference between the reference spectra of the baseline electrolyte and the PES-electrolytes. Due to the scarce amount of reference spectra of the various proposed PES-derived reduction products, only tentative assignments of the other bands can be made solely reliant on DFT-calculated vibrational modes performed by Jankowski et al. [98].

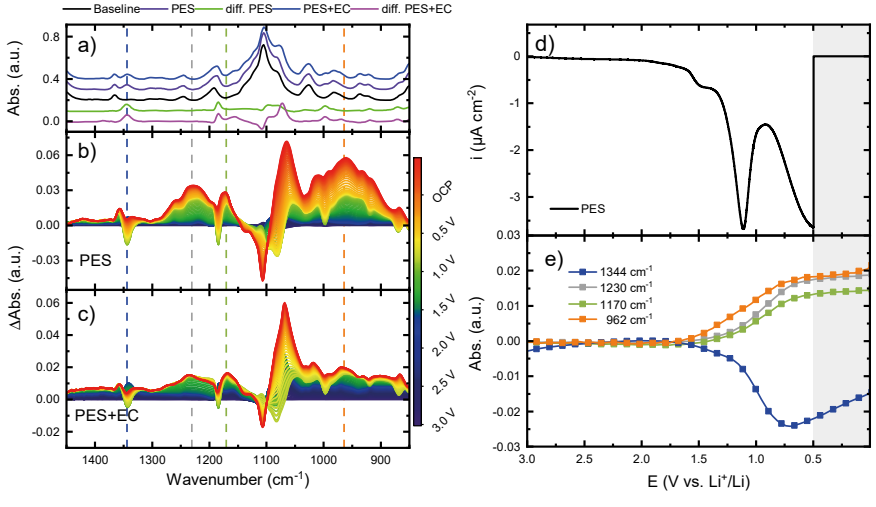

Figure 4.10. a) Absorbance spectra of the Baseline electrolyte with 5 wt.% PES, 5 wt. % PES+5 wt.% EC, and the difference spectra relative to the baseline spectrum. *Operando* ATR-FTIR absorbance spectra of a GC electrode in the b) PES- and c) PES+EC-electrolyte during a linear sweep voltammogram from the OCP to 0.5 V. d) Current response during polarisation from OCP to 0.5 V followed by OCP measurement and e) absorbance at selected wavenumbers in from the *operando* spectra of the PES-electrolyte.

No bands could be assigned to Li_2SO_3. The absence of Li_2SO_3 in the spectra, no clear propylene evolution and suppressed H_2 evolution point to that Li_2PES might only abstract one hydrogen radical or decompose without releasing gaseous species. The bands at 1170 and 962 cm^{-1} are assigned to $R(SO_3Li)_2$ and $R(OSO_2Li)_2$, respectively. These two species can be formed through dimerisation of two PES radicals which have been reduced by one electron each without the release of any other products. Such a scenario agrees well with the absence of gas evolution connected to PES-reduction. A simplified reaction without the intermediate radicals is shown as Reaction 4.16.

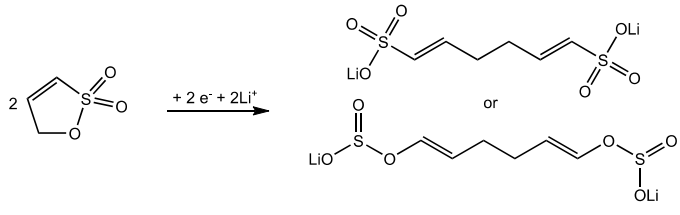

(4.16)

Both sulphur-based additives can form passivation layers on the electrode surface that are able to suppress EC reduction as no ethylene evolves at 0.8 V vs. Li^+/Li. An increase in H_2 evolution is observed in the DTD-electrolytes while a significant suppression is observed during PES reduction. In contrast to LiBOB in **Paper IV**, only the evolution of H_2 is suppressed. The current plateau at 1.6 V vs. Li^+/Li attributed to water reduction remains present. Furthermore, the PES reduction does not form any gaseous species. DTD reduction, on the other hand, produces a significant amount of ethylene. As shown in the EQCM measurement, DTD decomposes before the major reduction potential showcasing the instability of DTD towards reduced contaminants. The gas evolution and poor stability of DTD are problematic from an application point of view as handling the electrolyte and cells could cause an unwanted decomposition process before SEI formation cycling.

5 Conclusions and outlook

Obtaining fundamental understanding of electrode/electrolyte interphases is one of the greatest scientific challenges in the field of rechargeable batteries. Interphases stabilise the battery cell chemistries by separating the highly reactive electrodes from the electrolyte and are as such instrumental for battery lifetime and safety. Despite decades of research, interphases keep riddling the battery community because of their intricate formation/operation dynamics and complicated nm-sized multicomposite structures. Model systems adapted for dedicated *operando* analytical techniques were therefore developed and applied to reduce complexity and systematically explore the most well-recognised interphase in rechargeable batteries, namely the solid electrolyte interphase on the negative Li-ion battery electrode. Mechanistic insights into the formation and evolution of gaseous, soluble, and solid reaction products during SEI formation provide further pieces necessary not only to understand but also to guide the design of future rechargeable batteries of higher performance.

Model electrode/electrolyte systems were developed in a stepwise process with improvements targeting a few essential formation reactions at a time. The model system in **Paper I** consisted of a standard LIB electrolyte ($LiPF_6$ in EC:DEC) and a low-capacity glassy carbon negative electrode. From this study, a deeper understanding of the disparity between EC and PC as layer-forming solvents was obtained. Most notably, the reduction products of PC were evidenced to display significantly higher solubility, compared to EC, and provided as such much poorer passivating properties of the negative Li-ion electrode. In addition, clear effects of contaminants and hydrolysis of $LiPF_6$ salt and EC solvent on the SEI formation process were observed. In **Papers II** and **III**, $LiPF_6$ was therefore replaced with a less reactive salt ($LiClO_4$) and further insights into the reaction mechanism of EC and VC were obtained. Careful selection of electrolyte additives (such as VC) can provide thin and dense interphases as well as reduce the adverse influence of water impurities. Arguably, the most significant improvement of the model systems, as demonstrated in **Papers IV** and **V,** was employing a comparatively chemically inert electrolyte based on a low concentration of $LiClO_4$ in DME. The combination of this electrolyte with glassy carbon-based electrodes provided the most effective model electrode/electrolyte system investigated herein for the study of SEI formation.

Several essential aspects to consider when designing new electrolytes have been identified. All layer-forming molecular compounds studied herein, namely EC, VC, LiBOB, DTD and PES, passivate the electrode surface and suppress further electrolyte reduction. All layer-forming additives, or decomposition products thereof, are electrochemically reduced and passivate the electrode passivation at potentials above EC reduction at above 0.8 V vs. Li^+/Li. Suppression of EC reduction is key when tailoring the SEI composition as EC-derived species otherwise irreversibly form in larger amounts. While direct EC reduction may be suppressed, EC still partakes in the SEI formation driven by the additives, evidenced by the EC consumption at higher electrode potentials and the increased evolution of CO_2.

Based on the findings herein, it was concluded that an effective SEI exhibits a thickness of about 10 nm and consists likely of mostly inorganic compounds, such as lithium carbonate, lithium oxalate, lithium formate and lithium sulphate/sulphite compounds. A generally attractive property of an SEI former, as displayed by VC, is to suppress internal porosity by densifying the SEI. Water impurity reduction is a challenge and adversely influences SEI formation with unwanted chemical decomposition of electrolyte components, ultimately affecting cell performance. Despite extensive drying protocols to eliminate water from the systems, water finds its way, primarily demonstrated by H_2 in almost all OEMS measurements. Three different approaches to mitigate water reduction were demonstrated by VC, LiBOB and PES. VC was shown to scavenge water and its derivatives by suppressing the autocatalytic ring-opening reaction of EC while maintaining low SEI mass and resistance. Similarly, reduced PES showed the ability to abstract proton radicals from the electrode surface, significantly reducing the H_2 evolution. Reduction of LiBOB enabled a stable SEI at potentials above 1.6 V vs. Li^+/Li, thereby virtually eliminating water reduction and H_2 evolution.

This work identifies a critical need for further development of comprehensive reference spectral databases and models to fit experimental data. As showcased in **Paper V**, reference spectra of species derived from reduction of solvents and layer-forming additives are often absent in the literature, making characterisation challenging. The vast number of possible products from the solvents and additives used in LIBs results in almost uncountable SEI species combinations, thus synthesising all for reference experiments is impractical. Furthermore, the models used herein to fit EQCM-D do not account for the mixed mechanical properties of the SEI, as it is neither a fully rigid nor fully viscoelastic layer. Inadequate assignment of spectroscopic data and inaccurate models lead to information being lost. To fully utilise *operando* experimental data, development and implementation of advanced computational methods and models capable of simulating larger ensembles of electrolyte molecules and degradation products are required.

To conclude, extensive efforts in both academia and industry have been dedicated to improving the performance of LIBs through electrolyte

optimisation. While substantial knowledge exists within the field about which additive combinations enhance performance, much further fundamental scientific work still remains before the matters of this can be considered closed. The power of *operando* techniques and model systems to reveal SEI-related processes on a molecular level is demonstrated. Further development and refinement of *operando* analytical techniques, especially when combined with computational methods and models, clearly promise to provide the last pieces of the SEI puzzle and thereby the design keys to rechargeable batteries of longer lifetimes and higher safety.

Populärvetenskaplig sammanfattning

Under det senaste decenniet har den globala energikonsumtionen ökat från 161 000 TWh (2013) till 183 000 TWh (2023). Majoriteten av energin produceras av fossila bränslen. På grund av klimat och geopolitiska orsaker görs omfattande insatser för att minskade andelen energi som produceras från fossila bränslen. Detta genom att ersätta fossila bränslen med förnybara energikällor, så som sol- och vindkraft. Denna omställning ställer nya krav på energisystemet med avseende på energilagring för att kunna förse systemet med energi då solen inte lyser eller vinden inte blåser. Parallellt med denna omställning, görs liknande insatser inom transportsektor där förbränningsmotorer ersätts med elmotorer. Den mest lovande och utvecklade teknologin för att lösa dessa två utmaningar är litiumjonbatterier.

Litiumjonbatterier introducerades kommersiellt i början av 1990-talet och har sedan dess utvecklats och applicerats till den utsträckningen att pionjärerna inom fältet tilldelades Nobelpriset i kemi 2019. Ett litiumjonbatteri består av en positiv elektrod av metalloxider och en negativ elektrod av grafit. Dessa två material kan ta upp och släppa ifrån sig litiumjoner samtidigt som de tar upp eller släpper ifrån sig elektroner. Elektronerna färdas genom en yttre krets och kan användas för att driva elektroniska komponenter, till exempel en mobiltelefon. Litiumjonerna färdas genom elektrolyten som består vanligtvis av en blandning av organiskt lösningsmedel och litiumsalt. Då den positiva och negativa elektroden befinner sig vid höga respektive låga elektrokemiska potentialer vid uppladdning av batteriet bryts elektrolyten ned via oxidation eller reduktion. Produkterna från denna nedbrytning skapar ett passiverande lager på elektrodytan, detta lager förhindrar ytterligare nedbrytning. Den kemiska och fysikaliska egenskaper av dessa lager är avgörande för batteriets prestanda samt livslängd. För att styra och förbättra dessa passiverande lager, tillsätts additiv till elektrolyten vilka bryts ned innan eller tillsammans med lösningsmedlen och saltet. Optimering av prestanda och livslängd av litiumjonbatterier görs extensivt, dock ofta på applicerade system (”riktiga batterier”). Detta har resulterat i goda kunskaper om vilka additiv som förbättrar prestandan men för att kunna utveckla nya elektrolyter krävs förståelse av de underliggande processerna på fundamental nivå.

Målet med denna avhandling har varit att utforska och förstå nedbrytningen och bildandet av detta lager på den negativa elektroden, så kallade *the Solid Electrolyte Interphase,* SEI, på en fundamental nivå. SEI:et är väldigt tunt och

består av instabila molekyler vilket innebär att det reagerar, omvandlas och bryts ned så fort batteriet plockas isär för analys. För att kringgå detta har avancerade analysuppställningar utvecklats och dessa används för att studera bildandet och kompositionen av SEI:t i realtid utan att öppna upp batteriet, så kallat *operando*. Tre typer av *operando* analysuppställningar har använts under dessa studier, Online Electrochemical Mass Spectrometry (OEMS), *operando* Vibrational Spectroscopy (Raman och ATR-FTIR) och Electrochemical Quartz Crystal Microbalance with Dissipation monitoring (EQCM-D). Dessa tekniker kompletterar varandra vilket gör det möjligt att följa reaktionsprodukter i gasfas, lösning och fastfas under reduktionsprocesser av elektrolyten på elektrodytan. Kemin i ett litiumjonbatteri är komplex och många reaktioner sker samtidigt. För att kunna fokusera på och studera ett par av reaktionerna som har med SEI-bildandet att göra har modellsystem med noga utvalda elektrolyt/elektrod-kombinationer utvecklats och använts.

I **Artikel I** studerades skillnaden av de passiverande egenskaperna hos två snarlika lösningsmedel, EC och PC. EC är det lösningsmedel som möjliggjorde kommersialiseringen av litiumjonbatterier på grund av dess passiverande egenskaper. PC är ett annat lösningsmedel med mycket lik struktur jämfört med EC med saknar egenskapen att skapa ett effektivt passiverande SEI. I denna studie visades det att EC och PC genomgår identiska reduktionsprocesser men att produkterna hade väldigt skilda löslighet. SEI skapat av EC satt kvar på elektrodytan utan några tecken på upplösning medan SEI:t från PC var mycket tjockare och löste upp sig så fort PC slutade reduceras. Reduktionen av EC studerade mer djupgående i **Artikel II**. I bägge studier visades föroreningar, främst vatten, ha en tydlig negativ effekt på SEI-bildandet och elektrolyten.

VC, ett additiv som troligtvis finns i alla litiumjonbatterier, undersöktes i **Artikel III**. I denna studie visades det att en EC-baserad elektrolyt utan VC bildar ett tjockt SEI bestående av produkter till mesta dels från reaktioner mellan EC och hydroxidjoner från vattenreduktion. Med små mängder VC i elektrolyten, bildas ett tunt och tätt lager snabbt på elektrodytan vilket undertrycker vattenreduktionen avsevärt. I **Artiklarna IV** och **V** undersöktes tre ytterligare additiv, LIBOB, DTD och PES. Alla tre bildade ett passiverande SEI som undertrycker EC reduktion vilket kan vara till stor fördel då man försöker styra sammansättning och egenskaperna hos SEI:t.

Sammanfattningsvis har kombinationen av *operando* analysmetoder och modellsystem gett nya insikter om hur EC, VC, LiBOB, DTD och PES reduceras och bildar passiverande SEI på ett fundamentalt plan. Dessa insikter kan användas för att utveckla nya elektrolyt-sammansättningar för att förbättra prestanda och livslängden av litiumjonbatterier, vilket i sin tur möjliggör en hållbar framtid som är mindre beroende av fossila bränslen.

Acknowledgements

First and foremost, I would like to thank my supervisor, Erik J. Berg, for giving me the freedom to explore and try new ideas. You have guided me through this PhD project and helped me develop as a researcher. Secondly, I would like to acknowledge my co-supervisor, Leif Nyholm who introduced me to the field of electrochemistry and batteries, for which I will always be grateful. Thank you, Leif Edlén, for making all the custom-made cell parts. A big thank you to the Interphase group, both past and present members – Ville, Robin, Neeha, Casimir, Jackie, Viktor, Inti, Ziyin, Leiting, Xu, Paul, and Nataliia. Many thanks to Markus, Therese, Gustav, and Tatiana for great company during lunch and whenever there was time for beers. Many thanks go to Sarmad and Simon C for keeping the discussions at the fika table interesting. To all my colleagues at Structural and Inorganic Chemistry, thank you for making the department a wonderful workplace.

Special thanks to Robin, not only for being a great colleague but also a dear friend with an awesome family. You, Linn, Alva, and Alfons made the time outside of work great with first-rate playdates and weekly IKEA visits.

Tack mamma, pappa och Joanna. Ni har alltid stöttat mig och låtit mig göra det jag tycker är kul, ni är bäst.

Till sist, Maja och Agnes. Min familj. Ni gör vardagen fantastisk, utan er hade inget varit möjligt! Ett extra stort tack till Agnes för det fina omslaget till avhandlingen.

References

[1] H. Ritchie, P. Rosado, M. Roser, “Energy Production and Consumption,” Our World in Data. Accessed: Sep. 03, 2024. [Online]. Available: https://ourworldindata.org/energy-production-consumption

[2] A. Blakers, M. Stocks, B. Lu, C. Cheng, “A review of pumped hydro energy storage,” *Prog. Energy*, vol. 3, no. 2, p. 022003, 2021.

[3] T. Chen, Y. Jin, H. Lv, A. Yang, M. Liu, B. Chen, Y. Xie, Q. Chen, “Applications of Lithium-Ion Batteries in Grid-Scale Energy Storage Systems,” *Trans. Tianjin Univ.*, vol. 26, no. 3, pp. 208–217, 2020.

[4] Press release. NobelPrize.org, Nobel Prize Outreach AB, Accessed: Sep. 03, 2024. https://www.nobelprize.org/prizes/chemistry/2019/press-release/

[5] D. Deng, “Li-ion batteries: basics, progress, and challenges,” *Energy Sci. Eng.*, vol. 3, no. 5, pp. 385–418, 2015.

[6] K. Feng, M. Li, W. Liu, A. G. Kashkooli, X. Xiao, M. Cai, Z. Chen, “Silicon-Based Anodes for Lithium-Ion Batteries: From Fundamentals to Practical Applications,” *Small*, vol. 14, no. 8, p. 1702737, 2018.

[7] J. Liu, Z. Bao, Y. Cui, E. J. Dufek, J. B. Goodenough, P. Khalifah, Q. Li, B. Y. Liaw, P. Liu, A. Manthiram, Y. S. Meng, V. R. Subramanian, M. F. Toney, V. V Viswanathan, M. S. Whittingham, J. Xiao, W. Xu, J. Yang, X.-Q. Yang, J.-G. Zhang, “Pathways for practical high-energy long-cycling lithium metal batteries,” *Nat. Energy*, vol. 4, no. 3, pp. 180–186, 2019.

[8] K. Xu, “Electrolytes and Interphases in Li-Ion Batteries and Beyond,” *Chem. Rev.*, vol. 114, no. 23, pp. 11503–11618, 2014.

[9] K. Xu, “Nonaqueous liquid electrolytes for lithium-based rechargeable batteries,” *Chem. Rev.*, vol. 104, no. 10, pp. 4303–4417, 2004.

[10] D. Strmcnik, I. E. Castelli, J. G. Connell, D. Haering, M. Zorko, P. Martins, P. P. Lopes, B. Genorio, T. Østergaard, H. A. Gasteiger, F. Maglia, B. K. Antonopoulos, V. R. Stamenkovic, J. Rossmeisl, N. M. Markovic, “Electrocatalytic transformation of HF impurity to H_2 and LiF in lithium-ion batteries,” *Nat. Catal.*, vol. 1, no. 4, pp. 255–262, 2018.

[11] P. G. Kitz, P. Novák, E. J. Berg, “Influence of Water Contamination on the SEI Formation in Li-Ion Cells: An Operando EQCM-D Study,” *ACS Appl. Mater. Interfaces*, vol. 12, no. 13, pp. 15934–15942, 2020.

[12] R. Fong, U. von Sacken, J. R. Dahn, “Studies of Lithium Intercalation into Carbons Using Nonaqueous Electrochemical Cells,” *J. Electrochem. Soc.*, vol. 137, no. 7, pp. 2009–2013, 1990.

[13] C. L. Campion, W. Li, W. B. Euler, B. L. Lucht, B. Ravdel, J. F. DiCarlo, R. Gitzendanner, K. M. Abraham, “Suppression of toxic compounds produced in the decomposition of lithium-ion battery electrolytes,” *Electrochem. Solid-State Lett.*, vol. 7, no. 7, p. A194, 2004.

[14] K. Xu, M. S. Ding, S. Zhang, J. L. Allen, T. R. Jow, “An Attempt to Formulate Nonflammable Lithium Ion Electrolytes with Alkyl Phosphates and Phosphazenes,” *J. Electrochem. Soc.*, vol. 149, no. 5, p. A622, 2002.

[15] N. Gogoi, W. Wahyudi, J. Mindemark, G. Hernández, P. Broqvist, E. J. Berg, “Reactivity of Organosilicon Additives with Water in Li-ion Batteries,” *J. Phys. Chem. C*, vol. 128, no. 4, pp. 1654–1662, 2024.

[16] E. Peled, “The Electrochemical Behavior of Alkali and Alkaline Earth Metals in Nonaqueous Battery Systems—The Solid Electrolyte Interphase Model,” *J. Electrochem. Soc.*, vol. 126, no. 12, pp. 2047–2051, 1979.

[17] E. Peled, D. Golodnitsky, G. Ardel, “Advanced Model for Solid Electrolyte Interphase Electrodes in Liquid and Polymer Electrolytes,” *J. Electrochem. Soc.*, vol. 144, no. 8, pp. L208–L210, 1997.

[18] A. Zaban, D. Aurbach, “Impedance spectroscopy of lithium and nickel electrodes in propylene carbonate solutions of different lithium salts A comparative study,” *J. Power Sources*, vol. 54, no. 2, pp. 289–295, 1995.

[19] P. Verma, P. Maire, P. Novák, “A review of the features and analyses of the solid electrolyte interphase in Li-ion batteries,” *Electrochim. Acta*, vol. 55, no. 22, pp. 6332–6341, 2010.

[20] D. Aurbach, B. Markovsky, M. D. Levi, E. Levi, A. Schechter, M. Moshkovich, Y. Cohen, “New insights into the interactions between electrode materials and electrolyte solutions for advanced nonaqueous batteries,” *J. Power Sources*, vol. 81–82, pp. 95–111, 1999.

[21] P. Novák, D. Goers, L. Hardwick, M. Holzapfel, W. Scheifele, J. Ufheil, A. Würsig, “Advanced in situ characterization methods applied to carbonaceous materials,” *J. Power Sources*, vol. 146, no. 1–2, pp. 15–20, 2005.

[22] P. P. R. M. L. Harks, F. M. Mulder, P. H. L. Notten, “In situ methods for Li-ion battery research: A review of recent developments,” *J. Power Sources*, vol. 288, pp. 92–105, 2015.

[23] A. M. Tripathi, W.-N. Su, B. J. Hwang, “In situ analytical techniques for battery interface analysis,” *Chem. Soc. Rev.*, vol. 47, no. 3, pp. 736–851, 2018.

[24] A. J. Cowan, L. J. Hardwick, “Advanced Spectroelectrochemical Techniques to Study Electrode Interfaces Within Lithium-Ion and Lithium-Oxygen Batteries,” *Annu. Rev. Anal. Chem.*, vol. 12, no. 1, pp. 323–346, 2019.

[25] J. Maibach, J. Rizell, A. Matic, N. Mozhzhukhina, “Toward Operando Characterization of Interphases in Batteries,” *ACS Mater. Lett.*, vol. 5, no. 9, pp. 2431–2444, 2023.

[26] E. Goren, O. Chusid (Youngman), D. Aurbach, “The Application of In Situ FTIR Spectroscopy to the Study of Surface Films Formed on Lithium and Noble Metals at Low Potentials in Li Battery Electrolytes,” *J. Electrochem. Soc.*, vol. 138, no. 5, pp. L6–L9, 1991.

[27] M. Moshkovich, M. Cojocaru, H. E. Gottlieb, D. Aurbach, “The study of the anodic stability of alkyl carbonate solutions by in situ FTIR spectroscopy, EQCM, NMR and MS,” *J. Electroanal. Chem.*, 2001.

[28] R. Imhof, P. Novák, “In Situ Investigation of the Electrochemical Reduction of Carbonate Electrolyte Solutions at Graphite Electrodes,” *J. Electrochem. Soc.*, vol. 145, no. 4, pp. 1081–1087, 1998.
[29] F. Joho, P. Novák, “SNIFTIRS investigation of the oxidative decomposition of organic-carbonate-based electrolytes for lithium-ion cells,” *Electrochim. Acta*, vol. 45, no. 21, pp. 3589–3599, 2000.
[30] X. Zhang, J. K. Pugh, P. N. Ross, “Evidence for epoxide formation from the electrochemical reduction of ethylene carbonate,” *Electrochem. Solid-State Lett.*, vol. 4, no. 6, 2001.
[31] H. J. Santner, C. Korepp, M. Winter, J. O. Besenhard, K.-C. Möller, “In-situ FTIR investigations on the reduction of vinylene electrolyte additives suitable for use in lithium-ion batteries,” *Anal. Bioanal. Chem. 2004 3792*, vol. 379, no. 2, pp. 266–271, 2004.
[32] C. Korepp, H. J. Santner, T. Fujii, M. Ue, J. O. Besenhard, K. C. Möller, M. Winter, “2-Cyanofuran - A novel vinylene electrolyte additive for PC-based electrolytes in lithium-ion batteries,” *J. Power Sources*, vol. 158, no. 1, pp. 578–582, 2006.
[33] J. Yang, N. Solomatin, A. Kraytsberg, Y. Ein-Eli, “In-Situ Spectro-electrochemical Insight Revealing Distinctive Silicon Anode Solid Electrolyte Interphase Formation in a Lithium-ion Battery,” *ChemistrySelect*, vol. 1, no. 3, pp. 572–576, 2016.
[34] D. Alves Dalla Corte, G. Caillon, C. Jordy, J.-N. Chazalviel, M. Rosso, F. Ozanam, “Spectroscopic insight into Li-ion batteries during operation: An alternative infrared approach,” *Adv. Energy Mater.*, vol. 6, no. 2, p. 1501768, 2016.
[35] F. Shi, P. N. Ross, G. A. Somorjai, K. Komvopoulos, “The Chemistry of Electrolyte Reduction on Silicon Electrodes Revealed by in Situ ATR-FTIR Spectroscopy,” *J. Phys. Chem. C*, vol. 121, no. 27, pp. 14476–14483, 2017.
[36] M.-H. Shao, P. Liu, R. R. Adzic, “Superoxide Anion is the Intermediate in the Oxygen Reduction Reaction on Platinum Electrodes,” *J. Am. Chem. Soc.*, vol. 128, no. 23, pp. 7408–7409, 2006.
[37] J. P. Vivek, N. Berry, G. Papageorgiou, R. J. Nichols, L. J. Hardwick, “Mechanistic Insight into the Superoxide Induced Ring Opening in Propylene Carbonate Based Electrolytes using in Situ Surface-Enhanced Infrared Spectroscopy,” *J. Am. Chem. Soc.*, vol. 138, no. 11, pp. 3745–3751, 2016.
[38] J. P. Vivek, N. G. Berry, J. Zou, R. J. Nichols, L. J. Hardwick, “In Situ Surface-Enhanced Infrared Spectroscopy to Identify Oxygen Reduction Products in Nonaqueous Metal-Oxygen Batteries,” *J. Phys. Chem. C*, vol. 121, no. 36, pp. 19657–19667, 2017.
[39] M. Odziemkowski, M. Krell, D. E. Irish, “A Raman Microprobe In Situ and Ex Situ Study of Film Formation at Lithium/Organic Electrolyte Interfaces,” *J. Electrochem. Soc.*, vol. 139, no. 11, pp. 3052–3063, 1992.
[40] M. Inaba, H. Yoshida, Z. Ogumi, T. Abe, Y. Mizutani, M. Asano, “In Situ Raman Study on Electrochemical Li Intercalation into Graphite,” *J. Electrochem. Soc.*, vol. 142, no. 1, pp. 20–26, 1995.

[41] J. C. Panitz, F. Joho, P. Novák, "In situ characterization of a graphite electrode in a secondary lithium-ion battery using Raman microscopy," *Appl. Spectrosc.*, vol. 53, no. 10, pp. 1188–1199, 1999.

[42] P. Novák, F. Joho, R. Imhof, J. C. Panitz, O. Haas, "In situ investigation of the interaction between graphite and electrolyte solutions," *J. Power Sources*, vol. 81–82, pp. 212–216, 1999.

[43] S. Hy, Felix, Y. H. Chen, J. Y. Liu, J. Rick, B. J. Hwang, "In situ surface enhanced Raman spectroscopic studies of solid electrolyte interphase formation in lithium ion battery electrodes," *J. Power Sources*, vol. 256, pp. 324–328, 2014.

[44] Y. Ha, B. J. Tremolet de Villers, Z. Li, Y. Xu, P. Stradins, A. Zakutayev, A. Burrell, S.-D. Han, "Probing the Evolution of Surface Chemistry at the Silicon–Electrolyte Interphase via In Situ Surface-Enhanced Raman Spectroscopy," *J. Phys. Chem. Lett.*, vol. 11, no. 1, pp. 286–291, 2020.

[45] N. Mozhzhukhina, E. Flores, R. Lundström, V. Nyström, P. G. Kitz, K. Edström, E. J. Berg, "Direct Operando Observation of Double Layer Charging and Early Solid Electrolyte Interphase Formation in Li-Ion Battery Electrolytes," *J. Phys. Chem. Lett.*, vol. 11, no. 10, pp. 4119–4123, 2020.

[46] A. Gajan, C. Lecourt, B. E. Torres Bautista, L. Fillaud, J. Demeaux, I. T. Lucas, "Solid Electrolyte Interphase Instability in Operating Lithium-Ion Batteries Unraveled by Enhanced-Raman Spectroscopy," *ACS Energy Lett.*, vol. 6, no. 5, pp. 1757–1763, 2021.

[47] D. Aurbach, A. Zaban, "The application of EQCM to the study of the electrochemical behavior of propylene carbonate solutions," *J. Electroanal. Chem.*, vol. 393, no. 1–2, pp. 43–53, 1995.

[48] P. G. Kitz, M. J. Lacey, P. Novák, E. J. Berg, "Operando EQCM-D with Simultaneous in Situ EIS: New Insights into Interphase Formation in Li Ion Batteries," *Anal. Chem.*, vol. 91, no. 3, pp. 2296–2303, 2019.

[49] P. G. Kitz, M. J. Lacey, P. Novák, E. J. Berg, "Operando investigation of the solid electrolyte interphase mechanical and transport properties formed from vinylene carbonate and fluoroethylene carbonate," *J. Power Sources*, vol. 477, no. June, p. 228567, 2020.

[50] R. Imhof, P. Novák, "Degradation of mixed carbonate electrolytes on Li-ion battery graphite electrodesa. An in-situ study," *Proc. Symp. Batter. Portable Appl. Electr. Veh.*, vol. 97, no. 18, p. 313, 1997.

[51] B. D. McCloskey, D. S. Bethune, R. M. Shelby, G. Girishkumar, A. C. Luntz, "Solvents' Critical Role in Nonaqueous Lithium–Oxygen Battery Electrochemistry," *J. Phys. Chem. Lett.*, vol. 2, no. 10, pp. 1161–1166, 2011.

[52] N. Tsiouvaras, S. Meini, I. Buchberger, H. A. Gasteiger, " A Novel On-Line Mass Spectrometer Design for the Study of Multiple Charging Cycles of a Li-O_2 Battery ," *J. Electrochem. Soc.*, vol. 160, no. 3, pp. A471–A477, 2013.

[53] M. He, "Elucidating interface reactions in Li-ion batteries and supercapacitors by in situ gas analysis," PhD Thesis, ETH Zürich, 2016.

[54] R. Lundström, E. J. Berg, "Design and validation of an online partial and total pressure measurement system for Li-ion cells," *J. Power Sources*, vol. 485, p. 229347, 2021.

[55] P. Larkin, “Infrared and Raman Spectroscopy: Principles and Spectral Interpretation,” *Infrared Raman Spectrosc. Princ. Spectr. Interpret.*, pp. 1–228, 2011.
[56] P. E. Powers, *Field Guide to Nonlinear Optics*. SPIE, 2013.
[57] H. T. Kwon, C. M. Park, “Electrochemical characteristics of ZnSe and its nanostructured composite for rechargeable Li-ion batteries,” *J. Power Sources*, 2014.
[58] X. Liu, X. Y. Wu, B. Chang, K. X. Wang, “Recent progress on germanium-based anodes for lithium ion batteries: Efficient lithiation strategies and mechanisms,” *Energy Storage Mater.*, vol. 30, pp. 146–169, 2020.
[59] M. S. Schmidt, J. Hübner, A. Boisen, “Large Area Fabrication of Leaning Silicon Nanopillars for Surface Enhanced Raman Spectroscopy,” *Adv. Mater.*, vol. 24, no. 10, pp. OP11–OP18, 2012.
[60] J. Langer, D. J. de Aberasturi, J. Aizpurua, R. A. Alvarez-Puebla, B. Auguié, J. J. Baumberg, G. C. Bazan, S. E. J. Bell, L. M. Liz-Marzán, *et al.*, “Present and future of surface-enhanced Raman scattering,” *ACS Nano*, vol. 14, no. 1, pp. 28–117, 2020.
[61] D. Johannsmann, *The Quartz Crystal Microbalance in Soft Matter Research*. in Soft and Biological Matter. Cham: Springer International Publishing, 2015.
[62] G. Sauerbrey, “Verwendung von Schwingquarzen zur Wägung dünner Schichten und zur Mikrowägung,” *Zeitschrift für Phys.*, vol. 155, no. 2, pp. 206–222, 1959.
[63] Z. Yang, A. A. Gewirth, L. Trahey, “Investigation of fluoroethylene carbonate effects on tin-based lithium-ion battery electrodes,” *ACS Appl. Mater. Interfaces*, vol. 7, no. 12, pp. 6557–6566, 2015.
[64] V. Dargel, N. Shpigel, S. Sigalov, P. Nayak, M. D. Levi, L. Daikhin, D. Aurbach, “In situ real-time gravimetric and viscoelastic probing of surface films formation on lithium batteries electrodes,” *Nat. Commun.*, vol. 8, no. 1, p. 1389, 2017.
[65] X. Zhang, R. Kostecki, T. J. Richardson, J. K. Pugh, P. N. Ross, “Electrochemical and Infrared Studies of the Reduction of Organic Carbonates,” *J. Electrochem. Soc.*, vol. 148, no. 12, p. A1341, 2001.
[66] M. E. Spahr, T. Palladino, H. Wilhelm, A. Würsig, D. Goers, H. Buqa, M. Holzapfel, P. Novák, “Exfoliation of Graphite during Electrochemical Lithium Insertion in Ethylene Carbonate-Containing Electrolytes,” *J. Electrochem. Soc.*, vol. 151, no. 9, p. A1383, 2004.
[67] G. V. Zhuang, H. Yang, B. Blizanac, P. N. Ross, “A study of electrochemical reduction of ethylene and propylene carbonate electrolytes on graphite using ATR-FTIR spectroscopy,” *Electrochem. Solid-State Lett.*, vol. 8, no. 9, p. A441, 2005.
[68] H.-L. Zhang, C.-H. Sun, F. Li, C. Liu, J. Tan, H.-M. Cheng, “New Insight into the Interaction between Propylene Carbonate-Based Electrolytes and Graphite Anode Material for Lithium Ion Batteries,” *J. Phys. Chem. C*, vol. 111, no. 12, pp. 4740–4748, 2007.
[69] K. Xu, “Whether EC and PC Differ in Interphasial Chemistry on Graphitic Anode and How,” *J. Electrochem. Soc.*, vol. 156, no. 9, p. A751, 2009.

[70] N. Takenaka, Y. Suzuki, H. Sakai, M. Nagaoka, "On electrolyte-dependent formation of solid electrolyte interphase film in lithium-ion batteries: Strong sensitivity to small structural difference of electrolyte molecules," *J. Phys. Chem. C*, vol. 118, no. 20, pp. 10874–10882, 2014.

[71] C. Fang, J. Li, M. Zhang, Y. Zhang, F. Yang, J. Z. Lee, M.-H. Lee, J. Alvarado, M. A. Schroeder, Y. Yang, B. Lu, N. Williams, M. Ceja, L. Yang, M. Cai, J. Gu, K. Xu, X. Wang, Y. S. Meng, "Quantifying inactive lithium in lithium metal batteries," *Nature*, vol. 572, no. 7770, pp. 511–515, 2019.

[72] J. O. Besenhard, M. Winter, J. Yang, W. Biberacher, "Filming mechanism of lithium-carbon anodes in organic and inorganic electrolytes," *J. Power Sources*, vol. 54, no. 2, pp. 228–231, 1995.

[73] M. Moradzaman, G. Mul, "In Situ Raman Study of Potential-Dependent Surface Adsorbed Carbonate, CO, OH, and C Species on Cu Electrodes During Electrochemical Reduction of CO_2," *ChemElectroChem*, vol. 8, no. 8, pp. 1478–1485, 2021.

[74] M. Fujimoto, Y. Shouji, T. Nohma, K. Nlshio, "Charge-discharge characteristics of natural graphite electrode in some cyclic carbonates," *Vol. 65, Issue 11, Pages 949 - 953*, vol. 65, no. 11, pp. 949–953, 1997.

[75] D. Aurbach, K. Gamolsky, B. Markovsky, Y. Gofer, M. Schmidt, U. Heider, "On the use of vinylene carbonate (VC) as an additive to electrolyte solutions for Li-ion batteries," *Electrochim. Acta*, vol. 47, no. 9, pp. 1423–1439, 2002.

[76] J. C. Burns, R. Petibon, K. J. Nelson, N. N. Sinha, A. Kassam, B. M. Way, J. R. Dahn, "Studies of the Effect of Varying Vinylene Carbonate (VC) Content in Lithium Ion Cells on Cycling Performance and Cell Impedance," *J. Electrochem. Soc.*, vol. 160, no. 10, pp. A1668–A1674, 2013.

[77] M. Nie, J. Demeaux, B. T. Young, D. R. Heskett, Y. Chen, A. Bose, J. C. Woicik, B. L. Lucht, "Effect of Vinylene Carbonate and Fluoroethylene Carbonate on SEI Formation on Graphitic Anodes in Li-Ion Batteries," *J. Electrochem. Soc.*, vol. 162, no. 13, pp. A7008–A7014, 2015.

[78] B. Zhang, M. Metzger, S. Solchenbach, M. Payne, S. Meini, H. A. Gasteiger, A. Garsuch, B. L. Lucht, "Role of 1,3-Propane Sultone and Vinylene Carbonate in Solid Electrolyte Interface Formation and Gas Generation," *J. Phys. Chem. C*, vol. 119, no. 21, pp. 11337–11348, 2015.

[79] H. Ota, Y. Sakata, A. Inoue, S. Yamaguchi, "Analysis of Vinylene Carbonate Derived SEI Layers on Graphite Anode," *J. Electrochem. Soc.*, vol. 151, no. 10, p. A1659, 2004.

[80] S. Grugeon, P. Jankowski, D. Cailleu, C. Forestier, L. Sannier, M. Armand, P. Johansson, S. Laruelle, "Towards a better understanding of vinylene carbonate derived SEI-layers by synthesis of reduction compounds," *J. Power Sources*, vol. 427, pp. 77–84, 2019.

[81] K. U. Schwenke, S. Solchenbach, J. Demeaux, B. L. Lucht, H. A. Gasteiger, "The Impact of CO_2 Evolved from VC and FEC during Formation of Graphite Anodes in Lithium-Ion Batteries," *J. Electrochem. Soc.*, vol. 166, no. 10, pp. A2035–A2047, 2019.

[82] R. Lundström, N. Gogoi, T. Melin, E. J. Berg, "Unveiling Reaction Pathways of Ethylene Carbonate and Vinylene Carbonate in Li-Ion Batteries," *J. Phys. Chem. C*, vol. 128, no. 20, pp. 8147–8153, 2024.

[83] N. Gogoi, R. Lundström, G. Hernández, E. J. Berg, “Base-Driven Ring-Opening Reactions of Vinylene Carbonate,” *J. Electrochem. Soc.*, vol. 171, no. 5, p. 050506, 2024.

[84] Y. Mo, Y. Gofer, E. Hwang, Z. Wang, D. A. Scherson, “Simultaneous microgravimetric and optical reflectivity studies of lithium underpotential deposition on Au(111) from propylene carbonate electrolytes,” *J. Electroanal. Chem.*, vol. 409, no. 1–2, pp. 87–93, 1996.

[85] M. Martins, D. Haering, J. G. Connell, H. Wan, K. L. Svane, B. Genorio, P. Farinazzo, B. Dias Martins, P. P. Lopes, B. Gould, F. Maglia, R. Jung, V. Stamenkovic, I. E. Castelli, N. M. Markovic, J. Rossmeisl, D. Strmcnik, “Role of Catalytic Conversions of Ethylene Carbonate, Water, and HF in Forming the Solid-Electrolyte Interphase of Li-Ion Batteries,” *ACS Catal.*, pp. 9289–9301, 2023.

[86] L. Wang, A. Menakath, F. Han, Y. Wang, P. Y. Zavalij, K. J. Gaskell, O. Borodin, D. Iuga, S. P. Brown, C. Wang, K. Xu, B. W. Eichhorn, “Identifying the components of the solid–electrolyte interphase in Li-ion batteries,” *Nat. Chem.*, vol. 11, no. 9, pp. 789–796, 2019.

[87] S. Solchenbach, X. Huang, D. Pritzl, J. Landesfeind, H. A. Gasteiger, “Monitoring SEI Formation on Graphite Electrodes in Lithium-Ion Cells by Impedance Spectroscopy,” *J. Electrochem. Soc.*, vol. 168, no. 11, p. 110503, 2021.

[88] B. Han, Y. Zou, G. Xu, S. Hu, Y. Kang, Y. Qian, J. Wu, X. Ma, J. Yao, T. Li, Z. Zhang, H. Meng, H. Wang, Y. Deng, J. Li, M. Gu, “Additive stabilization of SEI on graphite observed using cryo-electron microscopy,” *Energy Environ. Sci.*, vol. 14, no. 9, pp. 4882–4889, 2021.

[89] S. Bolloju, N. Vangapally, Y. Elias, S. Luski, N. L. Wu, D. Aurbach, “Electrolyte additives for Li-ion batteries: classification by elements,” Jan. 01, 2025., *Pergamon*.

[90] U. Lischka, U. Wietelmann, M. Wegner, “German Patent DE 19829030 C1,” 1999.

[91] K. Xu, S. Zhang, B. A. Poese, T. R. Jow, “Lithium bis(oxalato)borate stabilizes graphite anode in propylene carbonate,” *Electrochem. Solid-State Lett.*, vol. 5, no. 11, pp. A259–A262, 2002.

[92] N. P. W. Pieczonka, L. Yang, M. P. Balogh, B. R. Powell, K. Chemelewski, A. Manthiram, S. A. Krachkovskiy, G. R. Goward, M. Liu, J. H. Kim, “Impact of lithium bis(oxalate)borate electrolyte additive on the performance of high-voltage spinel/graphite Li-ion batteries,” *J. Phys. Chem. C*, vol. 117, no. 44, pp. 22603–22612, 2013.

[93] J. Li, J. Yang, Z. Ji, M. Su, H. Li, Y. Wu, X. Su, Z. Zhang, “Prospective Application, Mechanism, and Deficiency of Lithium Bis(oxalate)Borate as the Electrolyte Additive for Lithium-Batteries,” *Adv. Energy Mater.*, vol. 13, no. 35, p. 2301422, 2023.

[94] G. V. Zhuang, K. Xu, T. R. Jow, P. N. Ross, “Study of SEI Layer Formed on Graphite Anodes in PC/LiBOB Electrolyte Using IR Spectroscopy,” *Electrochem. Solid-State Lett.*, vol. 7, no. 8, pp. A224–A227, 2004.

[95] B. T. Yu, W. H. Qiu, F. S. Li, G. X. Xu, “The electrochemical characterization of lithium bis(oxalato)borate synthesized by a novel method,” *Electrochem. Solid-State Lett.*, vol. 9, no. 1, p. A1, 2006.

[96] L. Madec, R. Petibon, J. Xia, J.-P. Sun, I. G. Hill, J. R. Dahn, "Understanding the Role of Prop-1-ene-1,3-Sultone and Vinylene Carbonate in $LiNi_{1/3}Mn_{1/3}Co_{1/3}O_2$/Graphite Pouch Cells: Electrochemical, GC-MS and XPS Analysis," *J. Electrochem. Soc.*, vol. 162, no. 14, pp. A2635–A2645, 2015.

[97] L. Madec, J. Xia, R. Petibon, K. J. Nelson, J.-P. Sun, I. G. Hill, J. R. Dahn, "Effect of Sulfate Electrolyte Additives on $LiNi_{1/3}Mn_{1/3}Co_{1/3}O_2$/Graphite Pouch Cell Lifetime: Correlation between XPS Surface Studies and Electrochemical Test Results," *J. Phys. Chem. C*, vol. 118, no. 51, pp. 29608–29622, 2014.

[98] P. Jankowski, N. Lindahl, J. Weidow, W. Wieczorek, P. Johansson, "Impact of Sulfur-Containing Additives on Lithium-Ion Battery Performance: From Computational Predictions to Full-Cell Assessments," *ACS Appl. Energy Mater.*, vol. 1, no. 6, pp. 2582–2591, 2018.

[99] D. S. Hall, J. P. Allen, S. L. Glazier, L. D. Ellis, L. Ma, J. M. Peters, I. G. Hill, J. R. Dahn, "The Solid-Electrolyte Interphase Formation Reactions of Ethylene Sulfate and Its Synergistic Chemistry with Prop-1-ene-1,3-Sultone in Lithium-Ion Cells," *J. Electrochem. Soc.*, vol. 164, no. 14, pp. A3445–A3453, 2017.

[100] J. Self, D. S. Hall, L. Madec, J. R. Dahn, "The role of prop-1-ene-1,3-sultone as an additive in lithium-ion cells," *J. Power Sources*, vol. 298, pp. 369–378, 2015.

Acta Universitatis Upsaliensis

Digital Comprehensive Summaries of Uppsala Dissertations from the Faculty of Science and Technology 2468

Editor: The Dean of the Faculty of Science and Technology

A doctoral dissertation from the Faculty of Science and Technology, Uppsala University, is usually a summary of a number of papers. A few copies of the complete dissertation are kept at major Swedish research libraries, while the summary alone is distributed internationally through the series Digital Comprehensive Summaries of Uppsala Dissertations from the Faculty of Science and Technology. (Prior to January, 2005, the series was published under the title "Comprehensive Summaries of Uppsala Dissertations from the Faculty of Science and Technology".)

Distribution: publications.uu.se
urn:nbn:se:uu:diva-540994

ACTA UNIVERSITATIS
UPSALIENSIS
2024